Naval Surface Warfare Center
Carderock Division
West Bethesda, Maryland 20817-5700

NSWCCD-TR-61-96/17 January 1997

Survivability, Structures and Materials Directorate
Research and Development Report

HIGH DAMPING STRUCTURAL MATERIALS

by

Catherine R. Wong

NSWCCD-TR-61-96/17 HIGH DAMPING STRUCTURED MATERIALS

REPORT DOCUMENTATION PAGE

Form Approved OMB No. 0704-0188

1. AGENCY USE ONLY (Leave blank)	2. REPORT DATE	3. REPORT TYPE AND DATES COVERED
	DECEMBER 1996	FINAL

4. TITLE AND SUBTITLE
HIGH DAMPING STRUCTURAL MATERIALS

5. FUNDING NUMBERS

6. AUTHOR(S)
Catherine Wong

7. PERFORMING ORGANIZATION NAMES(S) AND ADDRESSEE(S)
Naval Surface Warfare Center, Carderock Division
Code 612
Bethesda, Maryland 20817-5700

8. PERFORMING ORGANIZATION REPORT NUMBER
TR-61-96-17

9. SPONSORING/MONITORING AGENCY NAME(S) AND ADDRESS(ES)
Office of Naval Research (ONR 332)
6.2 Seaborne Materials Technology Block
800 North Quincy St.
Arlington, VA 22217-5660

10. SPONSORING/MONITORING AGENCY REPORT NUMBER

11. SUPPLEMENTARY NOTES
Program Element No. 61153N

12a. DISTRIBUTION/AVAILABILITY STATEMENT
Approved for public release: distribution is unlimited.

12b. DISTRIBUTION CODE

13. ABSTRACT (Maximum 200 words)

Damping capacity measurements on aluminum foam filled with epoxy confirmed previous finite element analysis which showed that a smaller phase size leads to lower damping.
Studies of high-temperature alloys in the Ti-Sn system based on the intermetallic compound Ti_3Sn have identified high damping alloys. The low frequency damping behavior shows loss factors as high as 0.04 at room temperature. The damping is a function of temperature and frequency but does not vary much with strain.
Zirconium and erbium modified Cu-Mn-Al was spray formed in an effort to increase homogeneity and damping capacity and decrease impurity levels. Although the microstructure revealed that the optimum spray forming parameters have not yet been achieved, the modified alloys showed both high damping and resistance to losing that damping capacity over time. The elemental additions also accelerated the formation of alpha manganese at the grain boundaries during aging.

14. SUBJECT TERMS

15. NUMBER OF PAGES

16. PRICE CODE

17. SECURITY CLASSIFICATION OF REPORT	18. SECURITY CLASSIFICATION OF THIS PAGE	19. SECURITY CLASSIFICATION OF ABSTRACT	20. LIMITATION OF ABSTRACT
Unclassified	Unclassified	Unclassified	Unclassified

ABSTRACT

Damping capacity measurements on aluminum foam filled with epoxy confirmed previous finite element analysis which showed that a smaller phase size leads to lower damping. Studies of high-temperature alloys in the Ti-Sn system based on the intermetallic compound Ti_3Sn have identified high damping alloys. The low frequency damping behavior shows loss factors as high as 0.04 at room temperature. The damping is a function of temperature and frequency but does not vary much with strain.
Zirconium and erbium modified Cu-Mn-Al was spray formed in an effort to increase homogeneity and damping capacity and decrease impurity levels. Although the microstructure revealed that the optimum spray forming parameters have not yet been achieved, the modified alloys showed both high damping and resistance to losing that damping capacity over time. The elemental additions also accelerated the formation of alpha manganese at the grain boundaries during aging.

ADMINISTRATIVE INFORMATION

This report was prepared as part of an investigation of the feasibility of using high damping alloys in Naval systems. It was sponsored by the Office of Naval Research as part of the Ship and Submarine Functional Materials Block Program from FY 91 through FY 96. The work was supervised by Dr. O. P Arora and Dr. L. Aprigliano CDNSWC Code 612. The work was performed under Progam Element 61153N.

ACKNOWLEDGMENTS

The author thanks R. C. Cammarata for his guidance, R. L. Fleischer for his initial work on the Ti-Sn material system, E. Graesser for his tutoring in mechanical systems, and L. Kabacoff of ONR for the funding which enabled us to do the low frequency damping measurements.
The author is indebted to Olin corporation for spray forming the CuMn material and to A. Chamberlain, A. Brandemarte, and R. Stockhausen for the metallographic services.

CONTENTS

FIGURES

TABLES

I. INTRODUCTION

A. Damping

Simply stated, damping is the dissipation of energy in vibrating systems which results in either the control of the amplitude of the oscillations or their eventual decay. Passive damping makes use of properties which are inherent to machinery or structural systems and which arise from energy dissipation taking place within stressed elements of vibrating components or from energy being imparted to a surrounding dissipative medium.

The science of passive damping is separated into two areas: material damping and mechanical damping. Damping in materials is caused by the movement of microstructural elements. These elements are, in order of increasing dissipative ability, point defects, line defects and domain walls. In metallic materials point defects include vacancies or interstitial elements; line defects are usually dislocations; and domain walls can separate twin, phase, or magnetic domains. In polymeric materials the damping is often due to rotation or sliding of long monomer chains. In mechanical damping the overall energy dissipation of the assembly is of interest and this can result from joints and dissipative devices (e.g. riveted joints with friction, viscous dampers, plastically deforming elements, viscoelastic layers) as well as damping due to interaction of the structure with its environment.

In material damping, two primary classes of materials are studied: metal alloys and polymers. Although some ceramics have been studied they have not been extensively explored. Each class has advantages and disadvantages as independent materials.

Generally speaking, polymers have excellent intrinsic damping capacities but suffer from poor stiffness, strength, and creep characteristics and also suffer from strongly temperature dependent material properties. Polymers are currently being used as a parasitic material to damp transverse vibrations in naval components. They generally exhibit highest damping near the glass transition temperature, Tg, which is frequency dependent, and are not structural materials. Often they must be used with a stiff constraining layer which further adds to the expense and weight of the component. They do not effectively damp longitudinal vibrations because they cannot be used to occlude the vibratory path.

Metals have good stiffness, strength, and creep characteristics. High damping alloys presently find very limited use in damping applications because their damping capacities are generally much lower than the peak damping of the polymers. They are intrinsically unstable due to the mobility of their microstructural elements and thermomechanical processing is critical to achieving high damping. Once achieved the damping capacity is relatively insensitive to temperature and frequency. They have sufficient structural properties to be fabricated into components; therefore, they are not parasitic and can damp longitudinal as well as transverse vibrations

Very little investigation has been made of ceramic materials. Vitreous enamels have been used as a damping coating at high temperatures[1].

The damping capacity is a unitless quantity and various measures of damping assume that the materials are homogeneous and linear. The most common measures are loss factor and specific damping capacity (SDC). Other common measures of damping capacity include the tangent of the phase lag (tan ϕ), damping ratio (ζ), inverse quality factor (Q^{-1}), and log decrement (δ). Each measure is based on a specific test method. By their inherent definitions, listed in Table 1, the measures of damping capacity listed above can be simply interrelated when damping levels are within the range $0 < \tan\delta < 0.14$. That is $Q^{-1} = \eta = \tan\phi = E'/E'' = \delta/\pi = \psi/2\pi = 2\zeta$.

These widely used interrelationships are approximations based on two simple anelastic models which are the Kelvin-Voigt (KV) model and the complex spring (CS) (which is equivalent to the Kimball-Lovell complex modulus model) [2,3,4] and an assumption of low damping. When higher levels of damping are of interest ($\tan\delta > 0.14$) the simple linear relationships given above can produce up to 40% error when converting from one damping measure to another and the conversions in Table 2 should be used.

Anelastic material behavior requires that the following conditions be imposed on stress, strain, and equilibrium in a material[3]:

Table 1. Damping Definitions

Damping Definitions	Remarks
Tangent of the Phase Lag $\tan\phi = \frac{k_2}{k_1}$ Complex Spring Model (CS) $\tan\phi = \frac{c\omega}{k} = 2\zeta\frac{\omega}{\omega_n}$ Kelvin-Voigt Model (KV)	$0 \le \phi < \frac{\pi}{2}$ k_1: elastic (or storage) modulus k_2: loss modulus c: damping coefficient k: elastic stiffness ω: frequency of harmonic input ζ: damping ratio ω_n: natural frequency
Specific Damping Capacity $\psi = \frac{\Delta W}{W}$	ΔW: the energy dissipated per cycle of harmonic steady state oscillation. W: a quantity representing energy storage during the oscillation (e.g. strain energy, elastic potential energy, kinetic energy, etc.)
Loss factor $\eta = \frac{\Delta W}{2\pi W}$	ΔW, W: are defined the same as above.
Inverse Quality Factor $Q^{-1} = \frac{\omega_2 - \omega_1}{\omega_n}$	$\omega_2 - \omega_1$: half-power bandwidth of the frequency response peak. ω_n: defined the same as above..
Logarithmic Decrement $\delta = \ln\frac{X_n}{X_{n+1}}$	X_n: The amplitude of a free decaying response after n cycles.

Table 2. Exact Conversions of Damping Measurements

Exact Conversions		Remarks
$\tan\phi = \frac{k_2}{k_1}$	CS	$0 \le \phi < \frac{\pi}{2}$
$\tan\phi = \frac{c\omega}{k} = 2\zeta\frac{\omega}{\omega_n}$	KV	
$\psi = 2\pi\tan\phi$	KV & CS	$0 \le \phi < \frac{\pi}{2}$ Relationship holds when $W = \frac{1}{2}kX_0^2$ where X_0 is the response amplitude of the oscillating steady state system either with or without inertia. or when $W = \left(\frac{1}{2}kx^2 + \frac{1}{2}m\dot{x}^2\right)$ for $\omega = \omega_n$ where x and $\dot{x}$ are the instantaneous position and velocity of the vibrating mass.
$\eta = \frac{\psi}{2\pi} = \tan\phi$	KV & CS	$0 \le \phi < \frac{\pi}{2}$ Relationship holds when W is defined as above
$Q_{CS}^{-1} = \sqrt{1+\tan\phi} - \sqrt{1-\tan\phi}$		$0 \le \tan\phi \le 1$ or $0 \le Q^{-1} \le \sqrt{2}$
$Q_{KV}^{-1} = \sqrt{1-2\zeta^2+2\zeta\sqrt{1+\zeta^2}} - \sqrt{1-2\zeta^2-2\zeta\sqrt{1+\zeta^2}}$		$0 \le \zeta \le .3535$ or $0 \le Q^{-1} \le \sqrt{1.5}$
$\delta = 2\pi\tan\frac{\phi}{2}$	CS	$0 \le \phi \le \frac{\pi}{2}$ or $0 \le \delta \le 2\pi$
$\delta = \frac{2\pi\zeta}{\sqrt{1-\zeta^2}}$	KV	$0 \le \zeta \le 1$ or $0 \le \delta \le \infty$

1) For each value of stress in a material there must be an equilibrium value of strain (as a corollary, this condition requires a complete recovery of strain upon unloading to zero stress).

2) The equilibrium response is arrived at after a time delay (self adjustment or relaxation).

3) A linear stress-strain relationship is required (linearity condition).

This definition differs from that of an ideally elastic material only in the condition imposed by item 2. For an ideally elastic material the equilibrium response is instantaneous; thus, the difference between an ideally elastic material and an anelastic material is based only on the condition of the ability of the material to respond instantaneously.

The condition of linearity is important to both the derivation and meaning of the measures of damping. This condition is satisfied by many materials subjected to low or moderate stresses (i.e. stresses much lower than the yield point). Linearity is embodied in the principle of superposition which states that when a sequence of stresses are applied to a material at different times the newly applied stress contributes to the resulting strain as though it were acting alone. In more specific terms this means that if there exists a stress history $\sigma_1(t)$ which produces a strain history $\varepsilon_1(t)$ and a separate stress history $\sigma_2(t)$ which produces a strain history of $\varepsilon_2(t)$ then the sum $\sigma_1(t) + \sigma_2(t)$ will produce a strain of $\varepsilon(t) + \varepsilon_2(t)$.

The loss factor, η or tan ϕ, (specific damping capacity, ψ) of a typical machinery system is on the order of 10^{-2} to 10^{-1} (6 to 60% ψ)[1]. Most structural metals have a loss factor on the order of 10^{-4} ($\psi < 1\%$)[5]. Therefore the effect of the damping capacity of most structural material on the damping capacity of the system is negligible. Structural polymer matrix composites reinforced with glass or graphite fiber have a loss factor on the order of 10^{-3} ($\psi < 1\%$) [6], which is still not enough to have much impact on the damping capacity of the structure. Additionally, since most systems have fewer joints when fabricated from these composites, the system loss factor for a structure made of composites is usually lower than the system loss factor for a structure made of metals. High damping structural materials have a loss factor on the order of 10^{-2} (> 6% ψ)[6], which has a measurable effect on the damping capacity of a machinery system. The loss factor of high damping viscoelastic (or viscous) material (e.g. polymeric and glassy materials) ranges from 10^{-1} to 10 (60 to 100% ψ)[5] when the temperature and frequency range is near the glass transition temperature. This allows a relatively small amount of material to make a large change in the damping capacity of the system. It should be noted that system loss factors can vary a great deal. When the system loss factors are low, materials with low loss factors can be useful. For example alloys with loss factors on the order of 10^{-3} have been patented to damp compact disc players as the players have quite low system loss factors.

High damping structural materials have the potential to greatly reduce vibration and noise in many types of mechanical systems. Mechanical systems experience two types of vibration; longitudinal and flexural. There are currently few effective methods to damp longitudinal vibrations in mechanical systems. Conventional damping treatments which are effective on flexural vibrations do not effectively attenuate longitudinal vibrations, because the damping material is not in the path of these vibrations. Fabrication of machinery systems from high damping material would be productive, but most structural materials, while having excellent stiffness and strength, possess poor damping properties. Conversely, polymers with very high damping capacities have neither the strength nor the stiffness for use as structural materials.

Three material systems are examined in this work.

•Reticulated open cell aluminum foam filled with epoxy. This is a hybrid metal polymer system where both phases are continuous.

•An intermetallic matrix of Ti_3Sn with regions of alpha Ti.

•A spray formed Cu Mn alloy with gettering element additions.

The damping capacity of these material systems was measured using a Dynamic Mechanical Thermal Analysis unit (DMTA) The DMTA uses a fixed-guided cantilevered test configuration shown in Figure 1. In this configuration, the clamp on the left holds the sample to a stationary frame while the clamp on the right attaches the sample to the controlled drive shaft. If slipping occurs between the sample and the clamps, erroneous

Figure 1. DMTA Test Setup

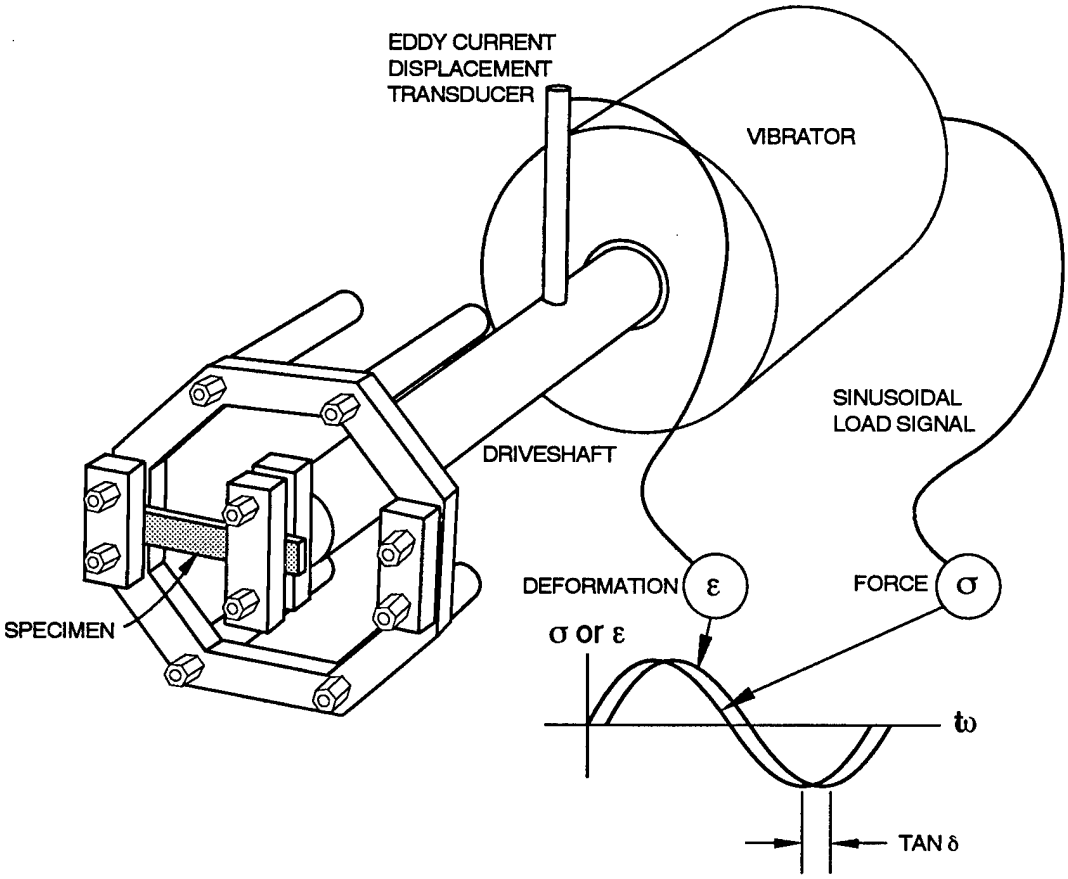

damping measurements can result. In order to minimize such errors, three-pronged clamps were used for the metal samples while flatter two pronged clamps were used for the more compliant Al-epoxy samples. A torque wrench was used to tighten the clamps in order to achieve consistent clamping. A torque of 60 cN-m was used for the metal samples and a torque of 20 was used for the samples which contained epoxy.

A small sinusoidal time-varying mechanical force is applied to the drive shaft and the displacement of the sample is measured. The phase angle, ϕ, of the lag between the

applied load and the measured displacement was calculated. The tangent of ϕ is a measureof the damping capacity commonly called the loss factor. The DMTA unit initially applies a high load which is then reduced until the specified displacement is achieved.

B. Al epoxy

When reticulated foams are filled with a viscoelastic material a composite with two continuous phases is made. The damping capacity and elastic modulus are some combination of the properties of the two materials. Although many models have been put forth to predict the modulus of composites, only a few cases have analytical solutions. For linear viscoelastic or anelastic material, when an analytical linear elastic solution exists the complex modulus can be substituted for the elastic modulus in the form7

$$k = k_1 + ik_2 \qquad \text{eq. 1}$$

where k is the complex modulus and k_1 and k_2 are defined in Table 1. The loss factor, η

$$\eta = \frac{k_1}{k_2} \qquad \text{eq. 2}$$

can be then be analytically found. Two specific cases which have analytic solutions are taken to be the upper and lower bounds. They are the Voigt or constant strain condition and the Reuss or constant stress condition. In both of these cases the composite is taken to be parallel phases of both materials. In the Voigt conditions the load is applied parallel to the phases so that all of the phases undergo the same strain. In the Reuss condition the

load is applied perpendicular to the phases so that all of the phases are subject to the same stress. The modulus, k, for the constant strain condition is

$$k_1 = k_1^{Al} V^{Al} + k_1^e V^e \qquad \text{eq. 3}$$

where k_1^{Al} and k_1^e are the elastic modulus of the Al and epoxy phases and V^{Al} and V^e are the volume fractions of Al and epoxy phases. Since this is an analytical solution the complex modulus can be substituted for the elastic modulus and using equation 1 equation 3 becomes

$$k = \left(k_1^{Al} + ik_2^{Al}\right)V^{Al} + \left(k_1^e + ik_2^e\right)V^e \qquad \text{eq. 4}$$

Substituting equation 2 into equation 4, separating into real and imaginary parts, and equating the imaginary sections of the equation yields

$$\eta = \frac{k_1^{Al}\eta^{Al}V^{Al} + k_1^e\eta^e V^e}{k_1^{Al}V^{Al} + k_1^e V^e} \qquad \text{eq. 5}$$

Similarly for the constant stress condition the elastic modulus is

$$\frac{1}{k_1} = \frac{V^{Al}}{k_1^{Al}} + \frac{V^e}{k_1^e} \qquad \text{eq. 6}$$

and again substituting the complex modulus for the elastic modulus, using equations 1 and 2 and solving for the loss factor by equating the imaginary parts we get

$$\eta = \frac{\eta^{Al}k_1^{Al}V^{Al}\left(1+\left(\eta^e\right)^2\right) + \eta^e k_1^e V^e\left(1+\left(\eta^{Al}\right)^2\right)}{k_1^{Al}V^e\left(1+\left(\eta^{Al}\right)^2\right) + k_1^e V^{Al}\left(1+\left(\eta^e\right)^2\right)} \qquad \text{eq. 7}$$

Where a composite falls between the constant stress and constant strain limits cannot be analytically predicted but composites have been modeled using finite element analysis(FEA)[8]. It was found that for the same volume fraction of Al the damping was higher when the epoxy was the matrix than when the Al was the matrix. Here matrix refers to the continuous phase. When the epoxy is the matrix, it can deform relatively freely which gives rise to high damping. When the epoxy is a discrete phase it can only deform to the extent that the stiffer Al allows, which results in lower damping. Additionally for a given volume fraction of Al the loss factor increased with increasing particle size. Damping measurements were made on epoxy filled Al foam samples to and compared to these FEA results. The samples were tested at two temperatures one above and one below the glass transition temperature at the test frequency. The epoxy exhibited markedly different moduli at these two temperatures so the effect of the difference between the modulus of the two phases in the composite could be evaluated.

C. Ti_3Sn

Two alloys in the Ti_3Sn intermetalic system have some unusual vibration transmission properties and a high melting temperature (1590 °C). The unusual properties came to light during the failure to determine elastic constants in high-frequency (5 to 20MHz) pulse-echo measurements[9]. Reflections from acoustic pulses could not be identified after a 1 cm travel distance in $Ti_{80}Sn_{20}$, $Ti_{78}Sn_{22}$, and $Ti_{75}Sn_{21}V_4$. The subscripts used here do not indicate different crystal structures but rather the overall composition of

the alloys. Subsequent work with the same technique[10] showed similar attenuation in $Ti_{72}Sn_{18}Al_{10}$ and in a different system, $Ti_{36}Cr_{54}Al_{10}$. Two binary compositions, Ti_3Sn and $Ti_{87}Sn_{13}$, that bracket those that showed the strong attenuation behaved normally in that their elastic constants could be determined. The damping capacity and mechanical properties of $Ti_{80}Sn_{20}$ and $Ti_{78}Sn_{22}$were measured in order to evaluate their potential as high damping structural materials. In both of these alloys the major phase is Ti_3Sn intermetallic and the minor phase is alpha Ti.

D. Cu Mn

Cu-Mn is a high damping alloy which has mechanical properties similar to bronze but dealloys even more readily[11]. Although the damping tends to decrease with time, the damping capacity was measured as relatively high in a full scale cast propeller after it had been in service[12]. High damping Cu-Mn alloys known as Incramute[i] and Sonoston,[ii] have been commercially produced and characterized, but the original commercial sources for these alloys are no longer available. Efforts by CanMet to cast Sonoston revealed difficulties in producing sound castings because of the reactivity of the Mn and because of the large differences in liquidus and solidus temperatures[13]. The castings often have a heavily-cored dendritic microstructure which results in a coarse banded microstructure

---

[i] Trademark, International Copper Research Association, Inc.

[ii] Trademark, Stone Manganese Marine, LTD.

upon hot working. Such microstructures are deleterious to both mechanical and corrosion properties. An effort by NRL to fabricate Cu-Mn alloys by rapid solidification processing (RSP) resulted in much better homogeneity but the damping capacity was very low[14]. It has been shown that an addition of 0.1 weight % of the rare earth element erbium (Er) to Incramute not only reduced the tendency of the Cu-Mn alloy to lose damping with time but also increased the damping by a factor of six and decreased the strain at which the damping mechanism became mobile[15]. Initial attempts to produce Er modified Incramute in 10 lb. ingots were not successful because of high impurity levels. The damping mechanism in Cu-Mn alloys is dependent on the movement of antiferromagnetic domain walls[16]. Solute elements diffuse to these walls causing them to become immobile. Er additions are thought to combine with the interstitial solute elements as well as Si and S, and reduce their diffusivity. The aging times in the RSP material were accelerated due to the enhanced solute migration kinetics of fine grained materials due to grain boundary diffusion. This enhanced solute migration would also reduce the damping. Spray forming Cu-Mn-Al was attempted to in order to produce a fine grain homogenous alloy and the addition of Er or Zr (a gettering element commonly used in copper alloy spray forming) was investigated to impart a durable high damping capacity.

II. EPOXY FILLED ALUMINUM FOAM HIGH DAMPING COMPOSITE

A. Experimental procedure

1. Preparation of samples

The samples were fabricated from 12% dense 10, 20 and 40 pore per inch aluminum foam produced by Energy Research and Generation Inc. from 6001 aluminum using a patented process. An organic reticulated foam was invested with an inorganic material which is inert to aluminum, such as plaster. When the plaster hardened the foam was dissolved leaving a mold of the foam. Molten metal was poured into this mold under vacuum and directionally solidified in order to insure complete infiltration of the mold. The plaster mold was then dissolved away leaving an open celled foam with nearly the same density and pore size as the original organic foam. The foam was given a T6 heat treatment. The foam was cut to the lengths shown in Table 3 and slowly compressed to 15 mm. The resulting densities are in Table 3. The compressed foam was put in a mold and liquid metallographic epoxy was poured in. The molds were set in a small vacuum chamber and a vacuum was drawn, the air pressure reapplied and the sample left to harden.

2. Damping capacity measurements

The samples were ground to 10 x 4 x 40 mm on a grinding wheel with 60 grit grinding paper. The epoxy was further cured at 80 °C for 4 hours. The damping measurements were made at 3 Hz with an 11 microns displacement and a maximum strain of $2x10^{-4}$.

Preliminary testing (Figure 2) showed that the epoxy exhibited a dramatic decrease in modulus by 80°C. The samples were tested at 30°C for one hour and then at 80°C for one hour. A minimum of 70 data points were taken at each temperature.

Table 3. Densities and Deformation History of Aluminum Foams

pores per inch before compression	initial length (mm)	final density %	time to compress (min.)	max. load (lb.)
10	15	12	31	340
20	15	12	34	280
40	15	12	33	470
10	20	16	60	690
20	20	16	30	690
40	20	16	61	510
10	31.25	25	53	810
20	31.25	25	80	1150
40	31.25	25	61	1150
10	62.3	50	207	4280
20	62.3	50	159	6020
40	62.3	50	226	5430

B. Results and discussion

The damping capacity and moduli of the monolithic materials are shown in Table 4. these values were used along with equations 5 and 7 to generate the curves in Figure 3 and Figure 4. The damping capacity of the composites, listed in Table 5, generally fall between the upper and lower bounds. It is evident that crushing the foam may have added a source of damping in the 10 and 20 PPI samples measured at 30°C. In general, however, the smaller the microstructure the lower the damping at both temperatures. It also appears that at 30°C where the damping capacity and modulus of each phase differed by an order of magnitude the resulting composite was near the constant stress curve, and

at 80°C where the damping capacity and modulus of each phase differed by two orders of magnitude the resulting composite was closer to the constant strain curve. The FEA[8] indicated that the stresses are higher in the stiffer Al phase whether Al is in the form of particles or matrix and the extent of the stress gradients depends on the volume fraction and particle size. The higher the gradient between the two phases, the less the more compliant epoxy is stressed. In a linear material the stress is proportional to the loss factor. Therefore since the stress is higher in the low damping Al than the high damping epoxy, the loss factor of the resulting composite is lower.

Figure 2. Loss Factor and Modulus of Epoxy at 1 Hz

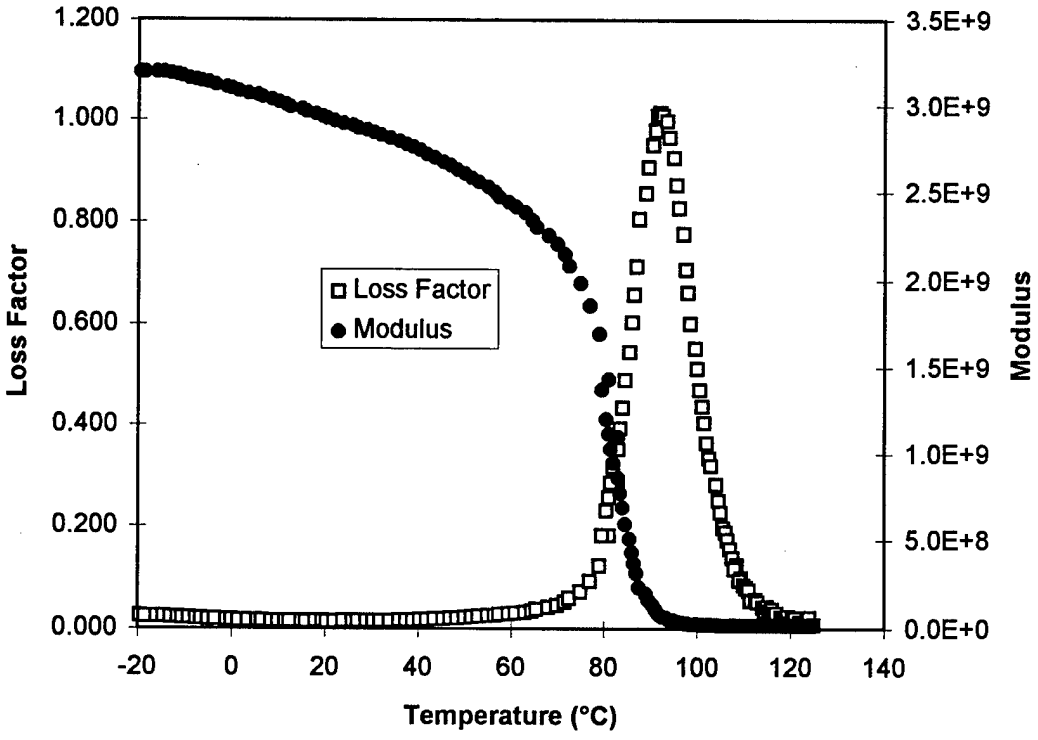

Table 4. Loss Factors and Moduli of Monolithic Materials

aluminum		epoxy measured at 30°C		epoxy measured at 80°C	
loss factor	modulus (Pa)	loss factor	modulus (Pa)	loss factor	modulus (Pa)
0.0045	6.70E+10	0.013	2.36E+09	0.647698	1.32E+08

Figure 3. Damping Capacity of Aluminum Epoxy Composites Measured at 30°C

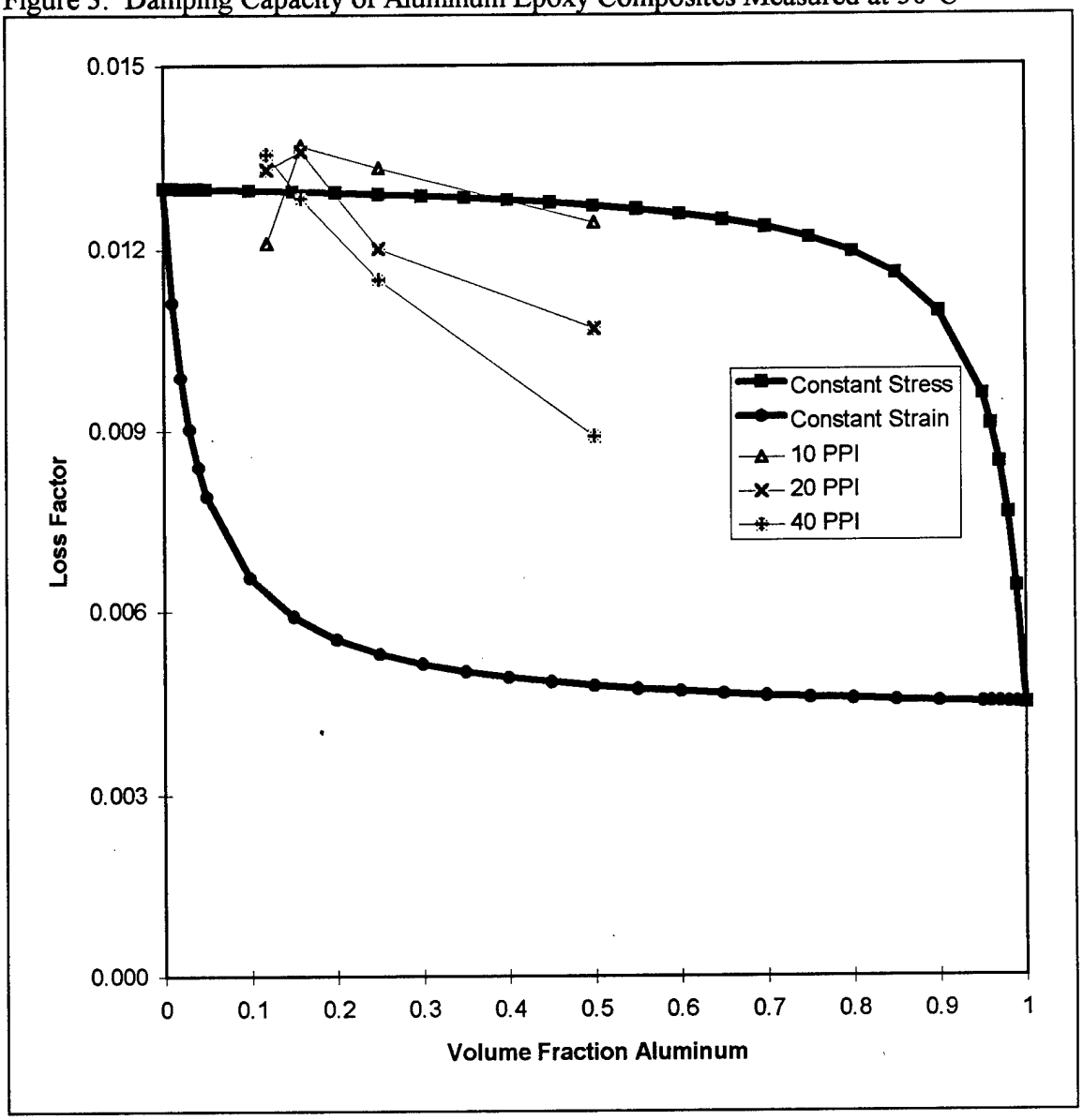

Figure 4. Damping Capacity of Aluminum Epoxy Composites at 80°C.

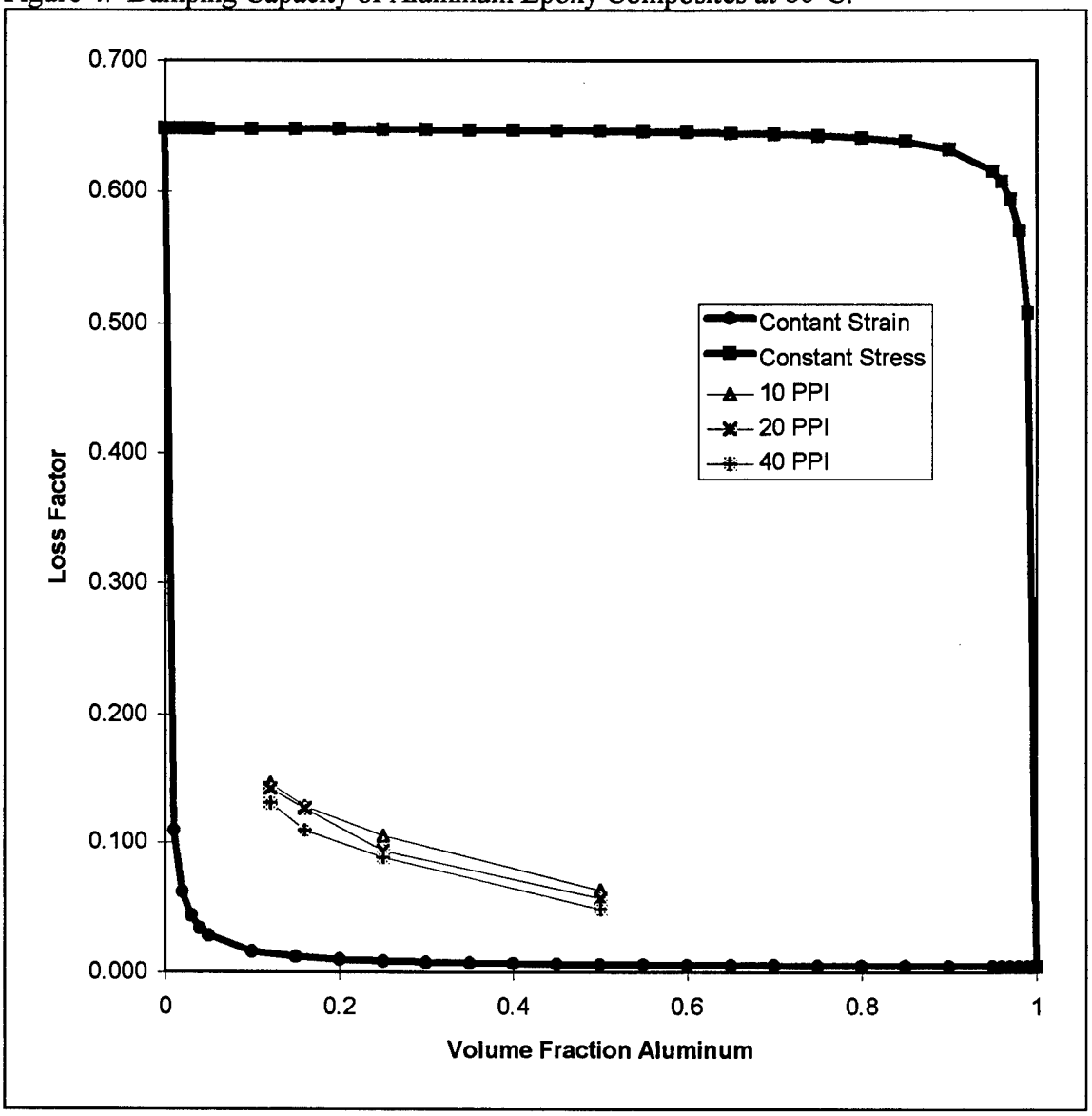

Table 5. Loss Factors for Aluminum-Epoxy Composites

volume fraction of aluminum	initial PPI	measurements at 30°C		measurements at 80°C	
		loss factor	standard deviation	loss factor	standard deviation
0.12	10	0.0121	0.000153	0.14673	0.006765
0.16	10	0.013691	0.000104	0.128816	0.00778
0.25	10	0.013333	0.000128	0.105011	0.00684
0.5	10	0.012437	0.000267	0.062749	0.003588
0.12	20	0.0133	0.000234	0.142678	0.008771
0.16	20	0.013594	0.000136	0.126991	0.007747
0.25	20	0.012014	0.000146	0.093572	0.005475
0.50	20	0.010689	0.000139	0.056678	0.003109
0.12	40	0.013553	0.000181	0.131143	0.00782
0.16	40	0.012833	0.000110	0.109505	0.00646
0.25	40	0.011496	0.00012	0.088068	0.005295
0.5	40	0.008905	0.000172	0.048373	0.002232

Although the FEA was two dimensional and thus not able to model a composite such as this with two continuous phases, it is clear that the unequal partitioning of the stress is still occurring. This effect is especially obvious in the case where the elastic modulus of the epoxy is low. In that case less of the stress can be taken up by the compliant epoxy and the damping capacity of the composite is closer to that of the monolithic Al. It is also evident that the scale of the microstructure changed the stress gradient and therefore the damping in a manner consistent with the FEA and this effect was also amplified by increasing the difference in elastic modulus between the two phases.

C. Conclusions

The damping capacity of the composite was found to be proportionally closer to that of the stiffer material when the difference in elastic modulus of the two materials was larger. This is likely due to the increased partitioning of the stress to the stiffer phase.

It was found that the damping capacity measurements on Al foam filled with epoxy confirmed previous finite element analysis which showed that a smaller phase size leads to lower damping. The larger the difference in elastic modulus the larger this effect was. This could have been due to and increasing stress gradient between the two phases of the composite.

D. Future work

Composites made with particulates which more closely follow the FEA model should be investigated in order to directly verify the model. Foams with increasing density should be made with thicker ligaments instead of by compacting in order to keep the pores per inch constant and quantify the effect of the pore size on the partitioning of the stress between the phases. Three dimensional modeling should be done to predict the behavior of composites with two continuous phases.

III. Ti_3Sn-BASED HIGH DAMPING ALLOYS

A. Experimental procedure

1. Preparation of samples

The initial samples of $Ti_{78}Sn_{22}$ and $Ti_{80}Sn_{20}$ were arc melted into disk-shaped ingots using titanium with a purity of 99.99% and tin with a purity of 99.999%. The results of the chemical analysis for interstitial elements are presented in Table 6. Samples were annealed at 1350 °C in Ar-filled SiO_2 ampoules that included a small piece of Y to getter oxygen. The resulting microstructure is shown in Figure 5.

The second batch of material was commercially cast in a 3" diameter ingot using commercial purity feed stock. The results of the interstitial analysis on the commercially cast material is in Table 6. Samples were annealed either at 1000°C for one hour in air, 1350°C for one hour in helium, or 1350°C for 20 hours in helium. The resulting microstructures are shown in Figure 6.

2. Damping capacity measurements

The initial samples for damping capacity testing were electro-discharge machined to approximately 4.0 x 1.0 x 0.1 cm. The second batch of material was cut to size using a diamond saw. The temperature dependence of the damping capacity was measured at 0.1,1, and 10 Hz with temperatures ramped from -30 °C to 100 °C at 1°C per minute. The strain was kept at 100 microstrain (maximum) and the frequencies were continually alternated. The run was then repeated to check for consistency. The dependence of the

damping capacity on the strain in the initial material was found by measuring the damping capacity at 25 °C while continually alternating the frequencies and periodically increasing the amplitude of the vibration. The reported values are the average of the damping capacity over thirty minutes. The strain dependence of the as-cast material was measured by repeating the temperature dependence test at increasing strain levels.

Figure 5. Microstructures of Initial TiSn Alloys

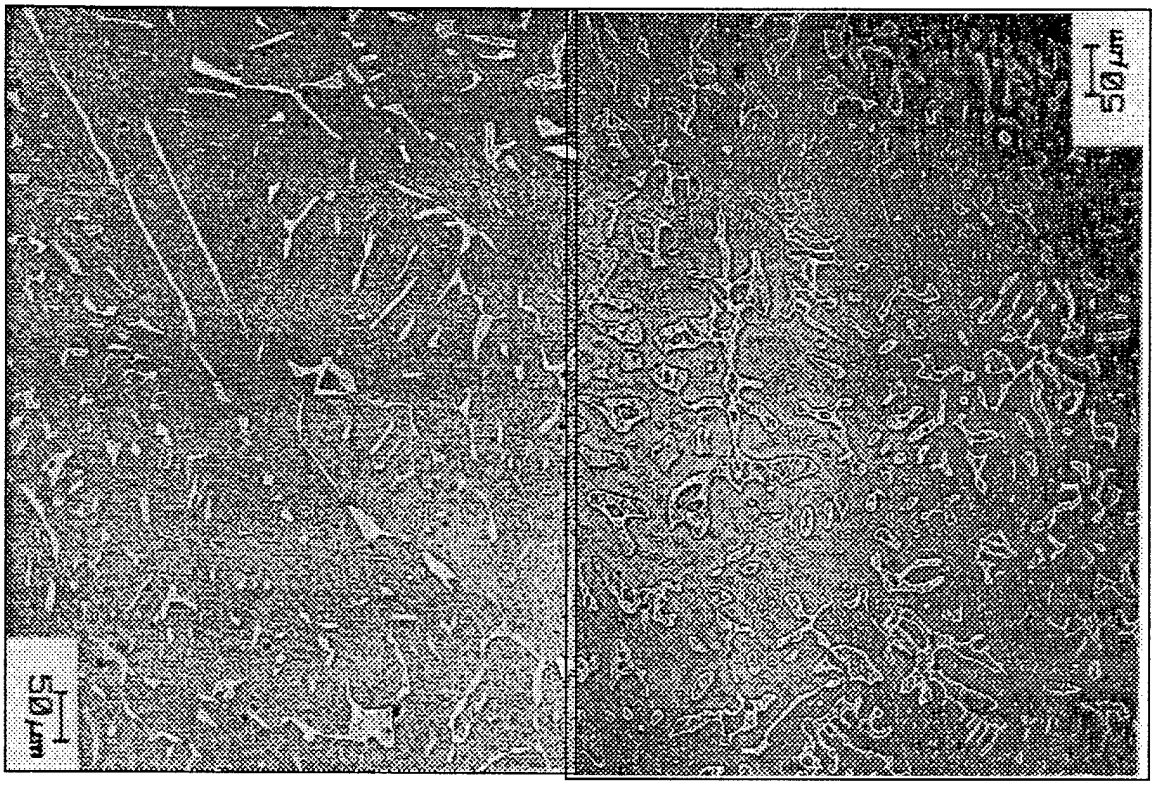

Initial $Ti_{78}Sn_{22}$ Initial $Ti_{80}Sn_{20}$

Figure 6. Microstructures of Commercially Cast TiSn Alloys.

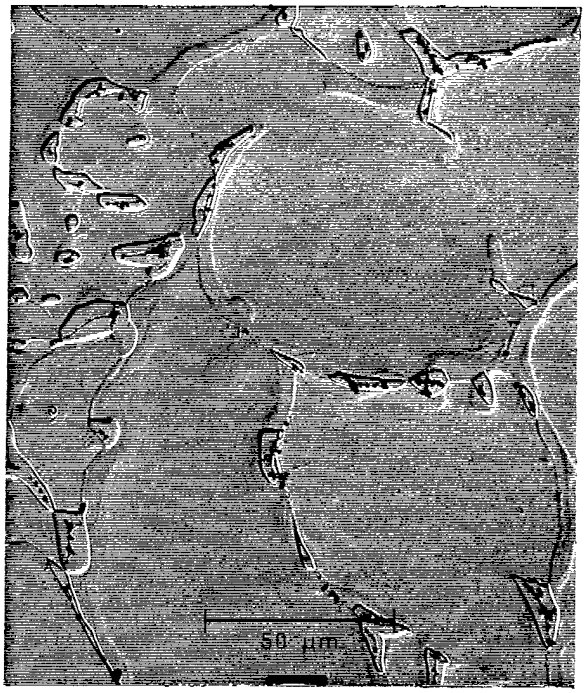

as- cast material

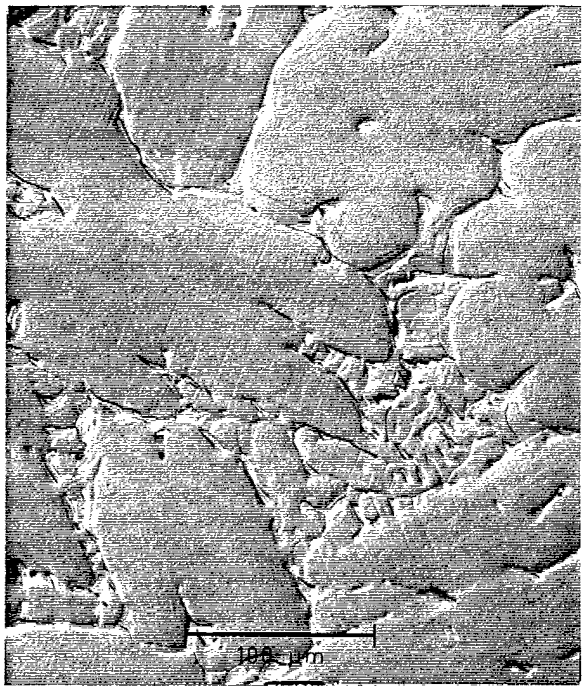

heat treated 1000°C for one hour

heat treated 1350°C for one hour

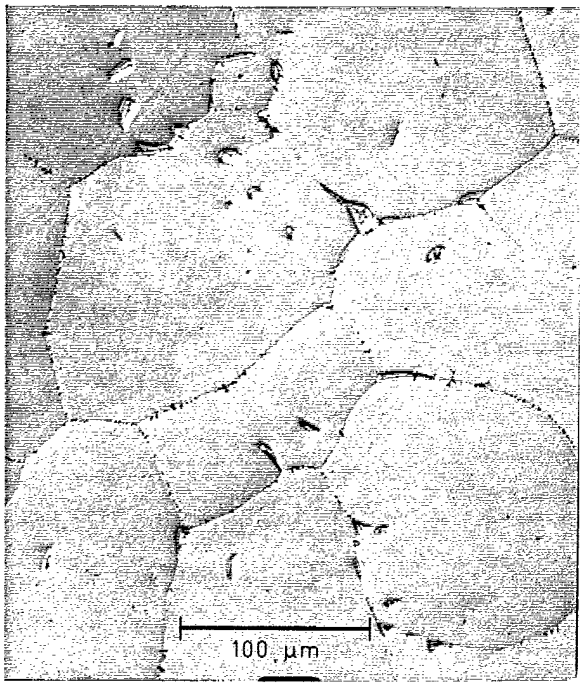

heat treated 1350°C for twenty hours

Table 6. Carbon, Nitrogen and Oxygen Analysis of TiSn Alloys.

material	C (wt ppm)	N (wt ppm)	O (wt ppm)
$Ti_{80}Sn_{20}$	100	15	500
$Ti_{78}Sn_{22}$	100	25	1000
commercially cast $Ti_{78}Sn_{22}$	100	122	.700

Corrections to the loss factors were made to account for the friction between the air and the moving sections of the DMTA, including the sample, as the sample was vibrated. The correction factor is frequency dependent, and for measured values of the loss factor below 0.01 it was necessary to correct the 10 Hz data. This was done by averaging the damping capacity values over a temperature range in which the loss factor was nominally flat. The average of the 1 Hz loss factor data was subtracted from the average of the 10 Hz loss factor data and that number was then subtracted from the 10 Hz loss factor values over the whole temperature range.

3. Materials characterization tests.

Standard 505 tensile specimens were used to determine tensile strength. Two of the samples were strain gauged and extensometers were used with all samples to measure the strain. Charpy V notch specimens were used to measure the toughness. The fracture surfaces were analyzed on a scanning electron microscope (SEM) and the chemical analysis were performed using energy dispersive spectroscopy (EDS)

B. Results and discussion

1. Damping

Damping capacity measurements shown in Figure 7 reveal a peak in the damping capacity as listed in Table 7. The amplitude of the damping capacity peaks decreased with increasing frequency in both samples. The data from the second runs on each sample closely repeat these values, as shown in Figure 8. The close agreement of the data from the two runs illustrates the lack of permanent change in the condition of the materials and the robustness of the damping. Since a discontinuity in the curve occurs near the damping capacity peak in the $Ti_{80}Sn_{20}$ in both runs of this sample it would be necessary to repeat that experiment in order to confidently define the damping capacity peak.

The damping curves for the cast material are shown in Figure 9-12 and the damping at 0.1 Hz is plotted in Figure 13 for all the alloys tested. Although the damping capacity for the as-cast material is similar to that of the initial material, it is evident that the heat treatments decreased the damping except for a slight increase in damping in the samples heated at 1350°C for 20 hours.

The plot of the strain dependence of the damping capacity shown in Figure 14 reveals an unexpected frequency dependence of the $Ti_{78}Sn_{22}$ sample. The loss factor decreases from 0.03 to 0.015 in the $Ti_{78}Sn_{22}$ sample as the strain increases from 50 to 1100 microstrain. Similarly in the $Ti_{80}Sn_{20}$ sample the loss factor decreases from 0.04 to 0.01 as the strain is increased from 50 to 500 microstrain, and the damping capacity at 10 Hz is

Figure 7. Damping Capacity for Initial Ti-Sn Alloys

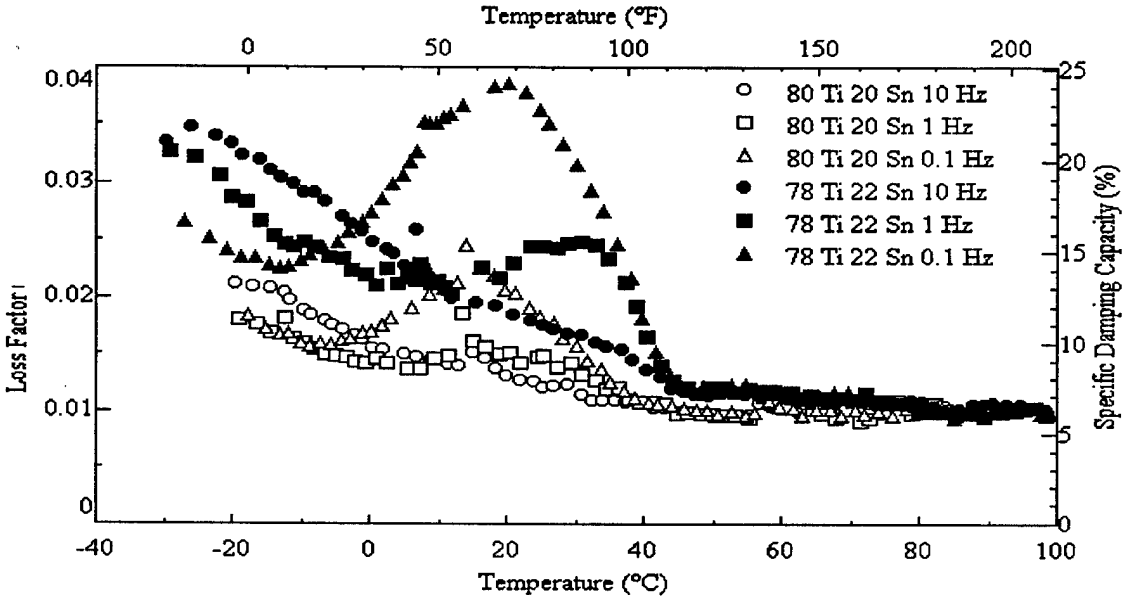

Figure 8. Duplicate Measurements of Damping Capacity for Initial Ti-Sn Alloys.

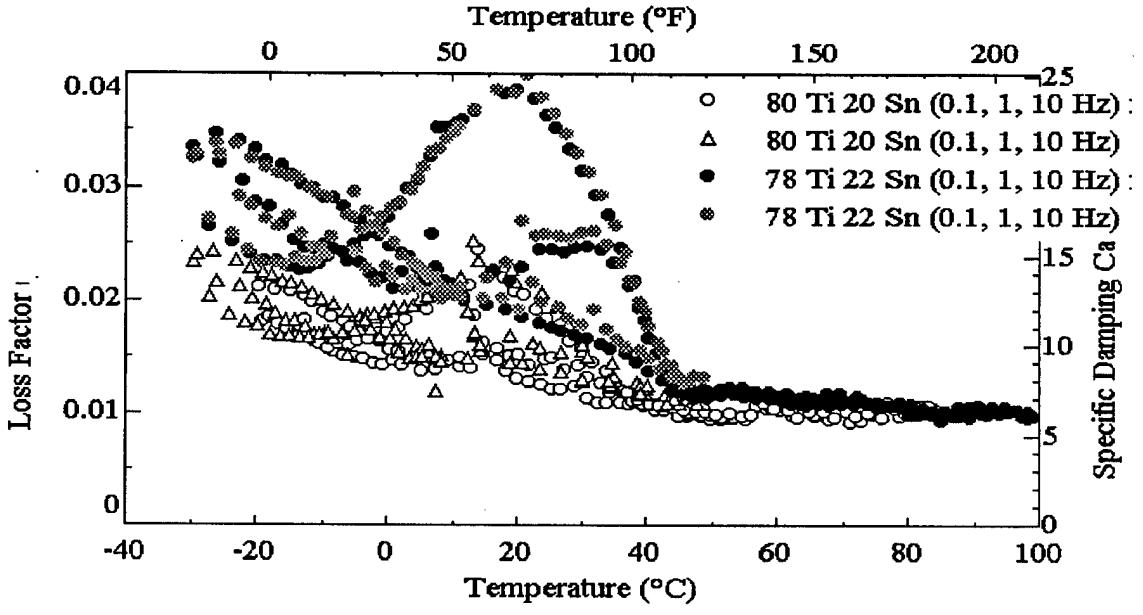

Table 7. Damping Peaks in TiSn Alloys.

Alloy	frequency	damping peak	
	(Hz)	loss factor	temperature (°C)
$Ti_{78}Sn_{22}$	0.1	0.04	20
	1		30
	10	0.017	35
$Ti_{80}Sn_{20}$	0.1	025	15
	1		15
	10	0.015	15
Cast $Ti_{78}Sn_{22}$ as-cast	0.1	0.026	17
	1	0.017	0-26
1000°C for one hour	0.1	0.017	10
	1	0.011	20
1350°C for one hour	0.1	0.014	8
1350°C for one hour	0.1	0.014	8

Figure 9. Damping Capacity of As-Cast $Ti_{78}Sn_{20}$

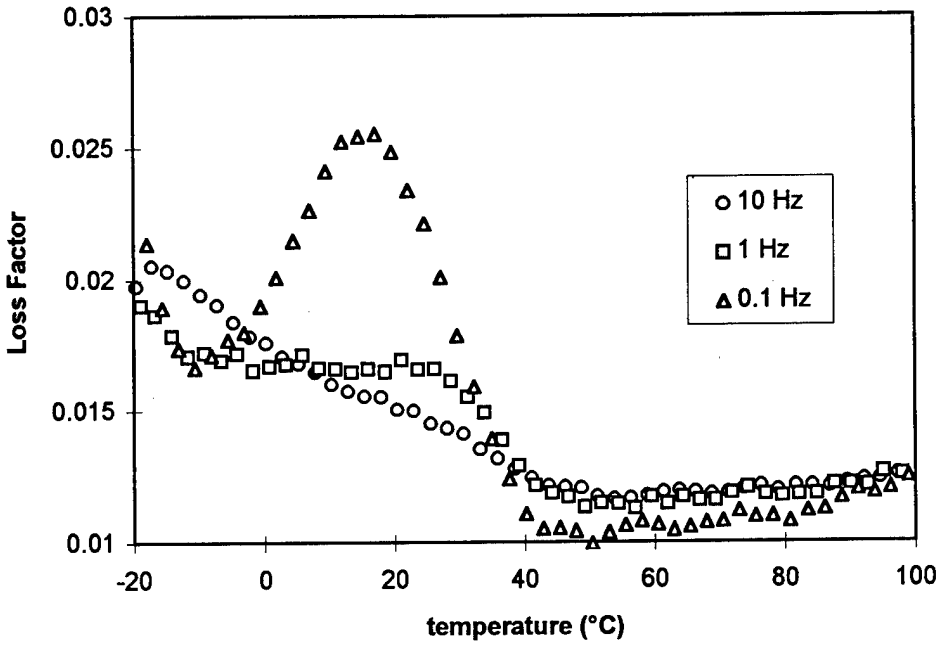

Figure 10. Damping Capacity of $Ti_{78}Sn_{22}$ Heat Treated at 1000°C for One Hour

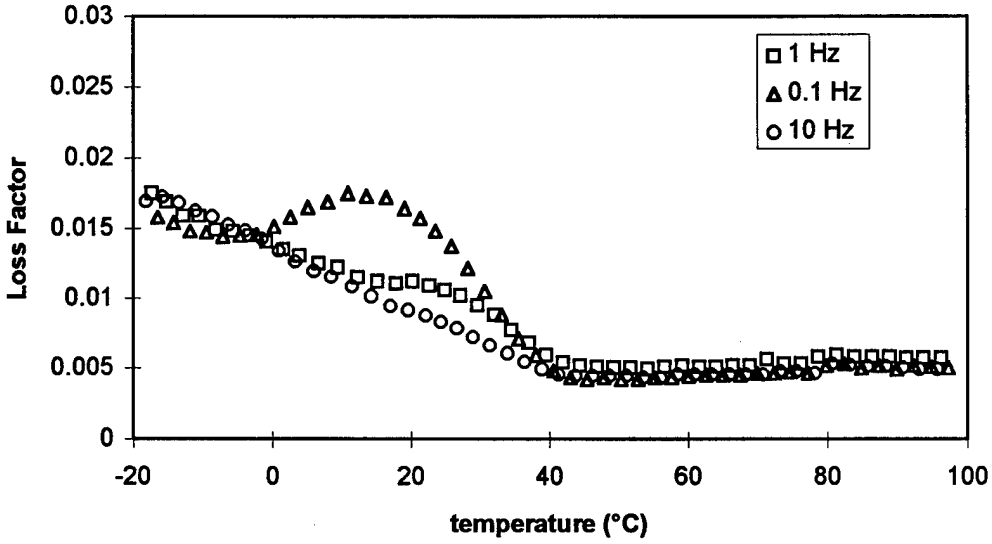

Figure 11. Damping Capacity of Ti78Sn22 Heat Treated at 1350°C for One Hour

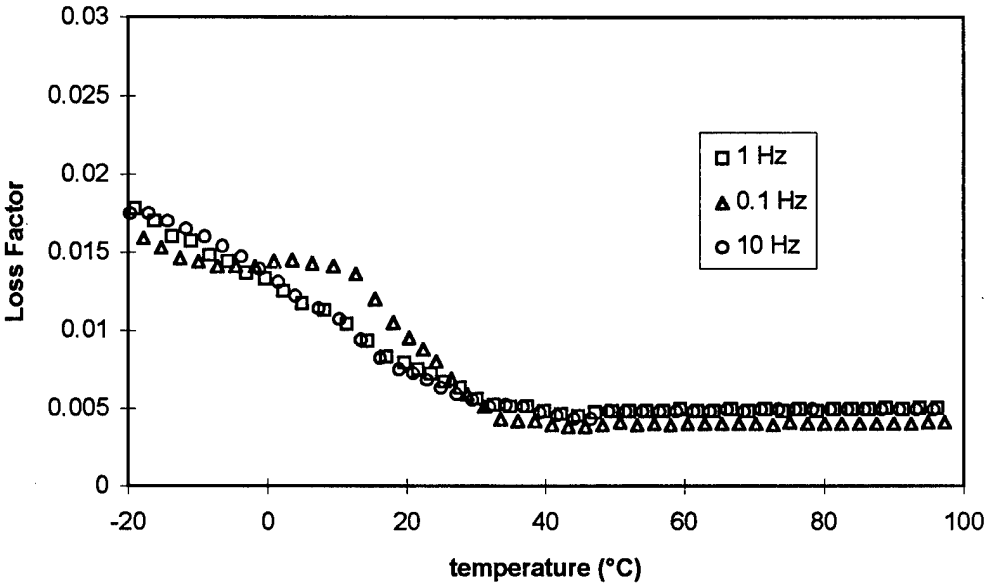

Figure 12. Damping Capacity of $Ti_{78}Sn_{22}$ Heat Treated at 1350°C for 20 Hours

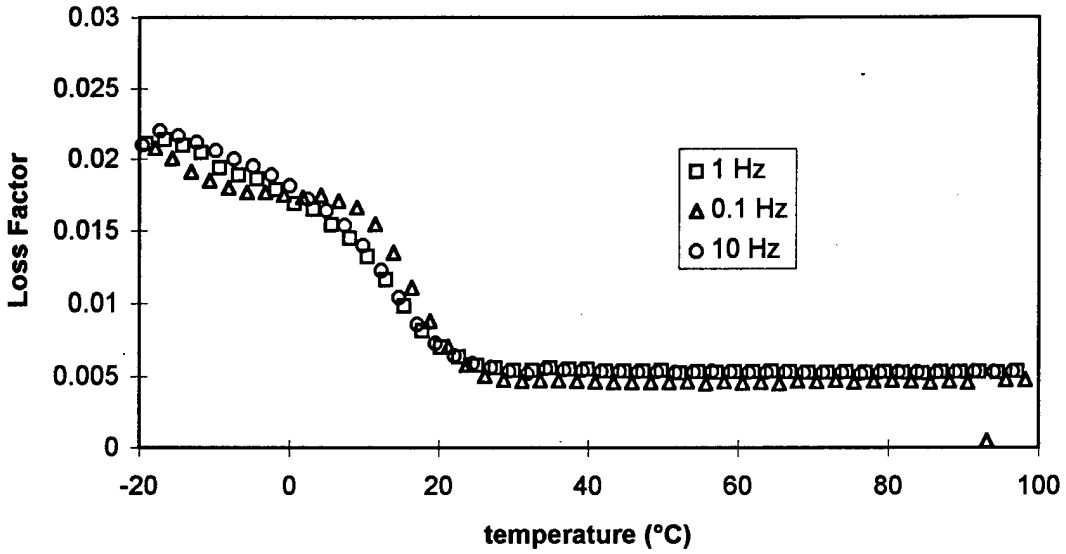

Figure 13. Damping Capacity of Ti-Sn alloys at 0.1 Hz and 100 microstrain.

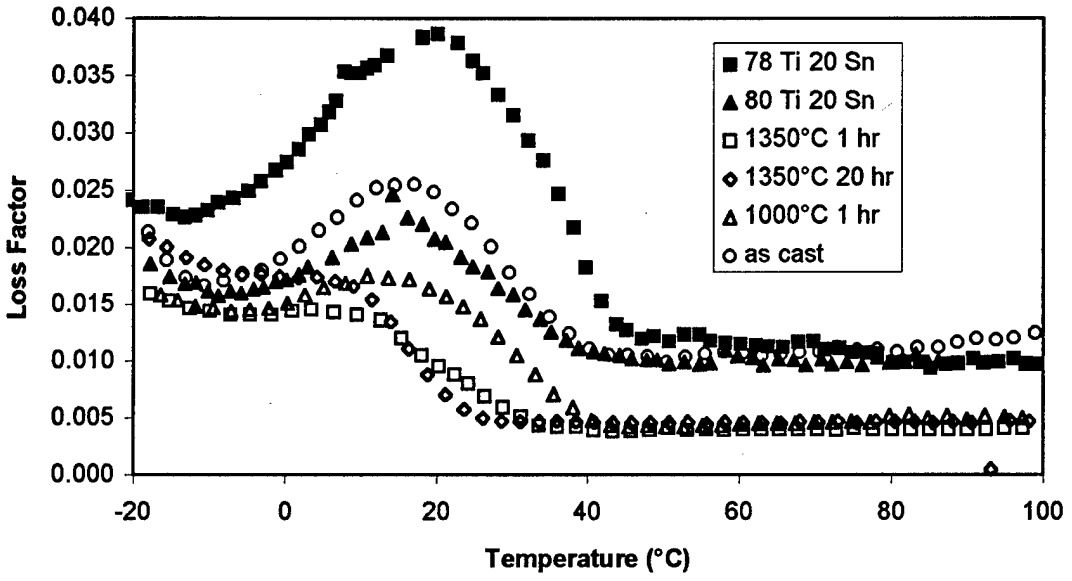

Figure 14. Strain Dependence of Initial Ti-Sn Alloy at 25°C

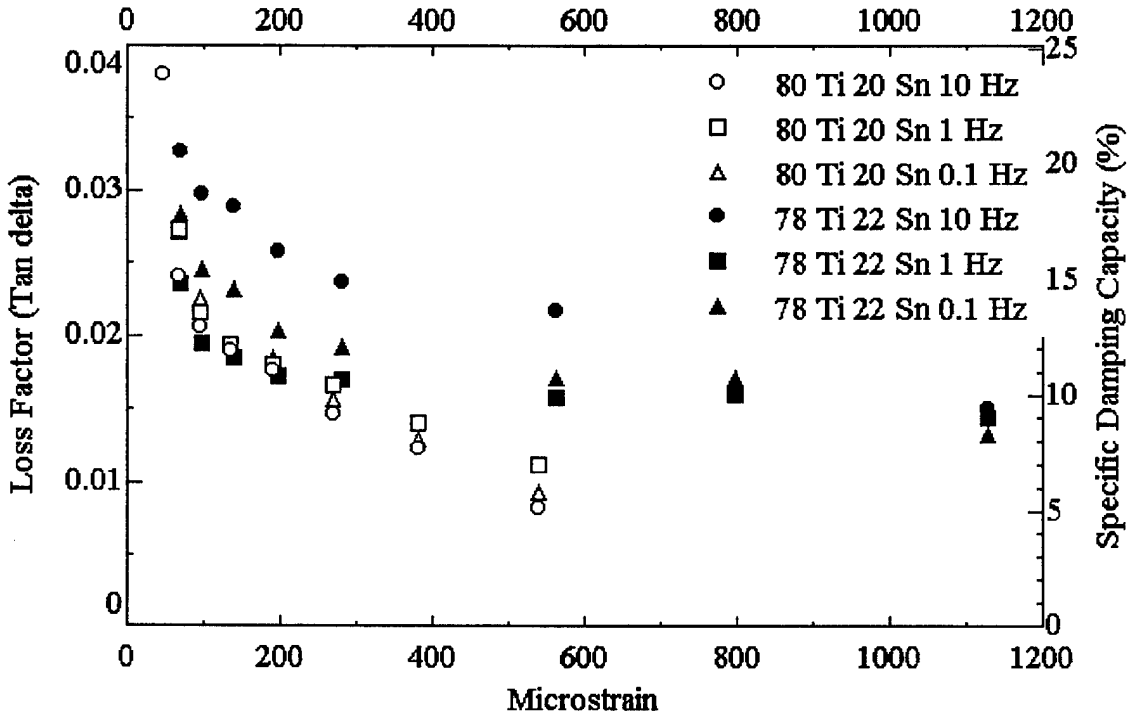

always higher than the damping capacity at other frequencies. This implies that 25 °C (the temperature at which the strain dependence was measured) is higher than the relaxation peak temperature for 0.1 and 1 Hz and below the peak temperature for 10 Hz. This is not confirmed by the temperature scan data. The plot of the strain dependence of the Ti80Sn20 sample in Figure 15 shows very little frequency or strain dependence, especially at higher strains. Figure 16 shows that the strain dependence of the damping capacity of the as-cast material is affected by temperature only up to 200 microstrain.

Figure 15. Strain Dependence of the Damping Capacity of As-Cast $Ti_{78}Sn_{22}$ at 25°C

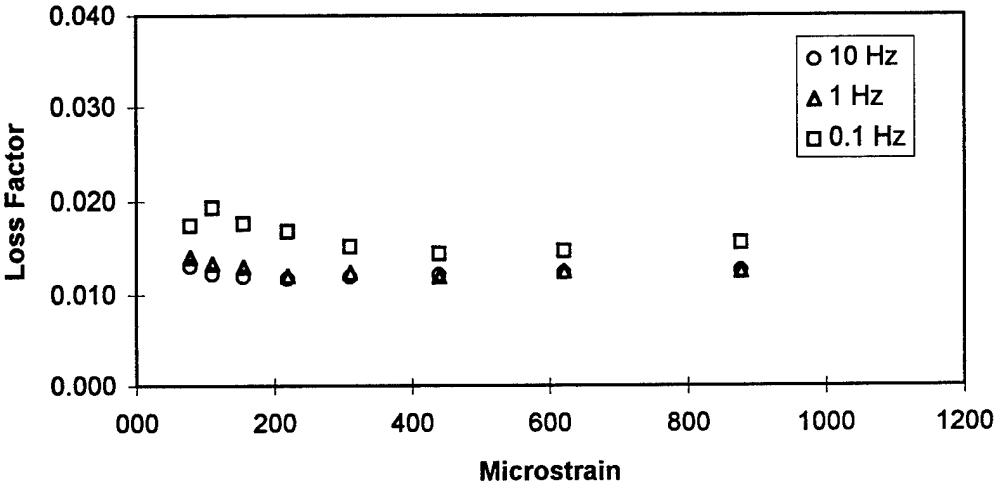

2. Mechanical property results

The results of the tensile tests are presented in Table 8. The strength and ductility were very low. Similarly, the results of the Charpy-V-Notch tests were all under one ft-lb. The average Young's modulus of the five tests measured by extensometer and strain gauge was 0.3 GPa with a standard deviation of 0.03. The modulus measured in the DMTA was about 1.2 GPa. This contrasts with ultrasonic modulus measurements of similar alloys containing a Ti_3Sn intermetallic matrix with a dispersed alpha Ti phase. While the commercially cast material in this study contained about 89% intermetallic phase (as calculated from composition), a $Ti_{75}Sn_{25}$ alloy which contained 100% intermetallic

phase had a modulus of 207 GPa and a $Ti_{87}Sn_{13}$ alloy which contained about 53% intermetallic phase had a modulus of 121 GPa[10].

Figure 16. Strain Dependence of the Damping Capacity of As-Cast $Ti_{78}Sn_{22}$ as a Function of Temperature.

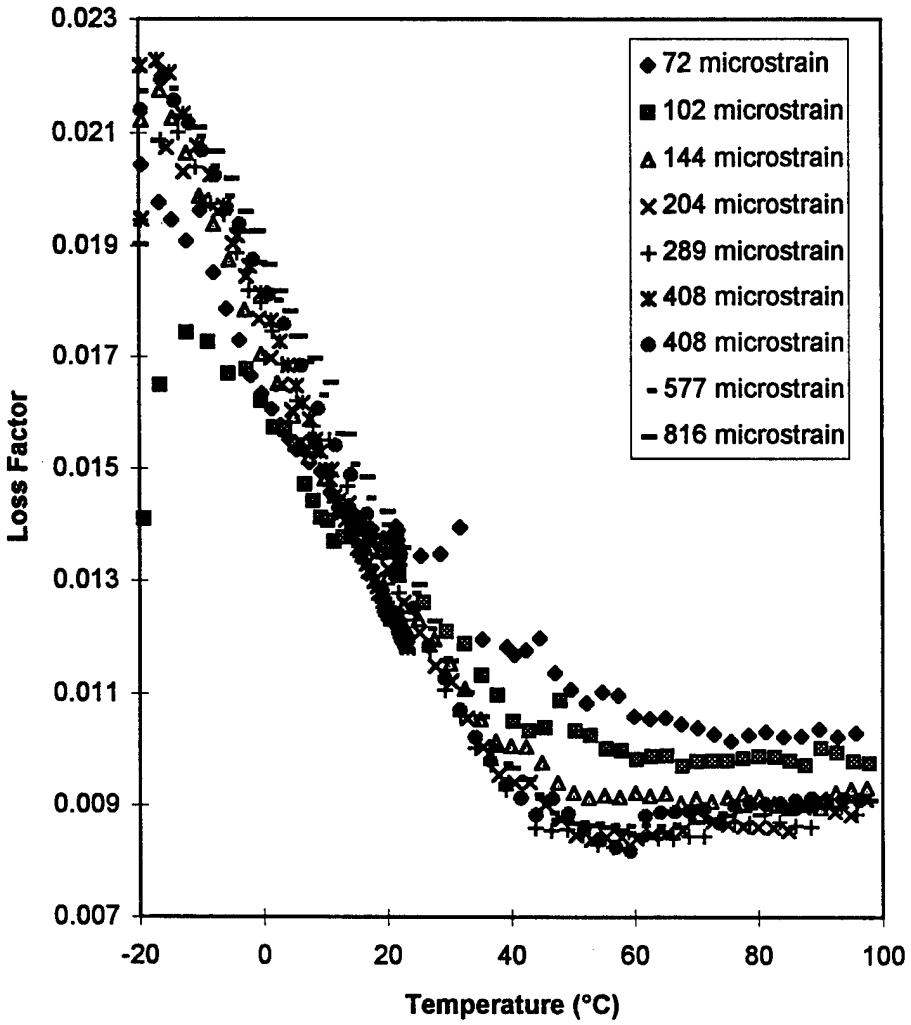

Table 8. Mechanical Properties of As-cast $Ti_{78}Sn_{22}$

test sample	ultimate tensile strength (MPa)	reduction in area (%)	elongation (%)
1	1.3	2.3	0.38
2	1.4	1.6	0.45
3	1.4	2.0	--
5	1.4	0.0	0.39
6	1.0	1.2	0.36

The micrographs reveal that the microstructure of all the alloys examined in this study contained two phases. The majority phase was always intermetallic Ti_3Sn and the minor phase alpha Ti. In the initial samples the alpha Ti phase is discrete and dispersed while in the commercially cast material it forms an almost continuous phase lining the grain boundaries. SEM micrographs of the fracture surfaces, like that shown in Figure 17, show that the fractures occurred primarily along the grain boundaries through the alpha phase.

C. Conclusions

Two alloys, $Ti_{78}Sn_{22}$ and $Ti_{80}Sn_{20}$ have high damping from 0.1 to 10 Hz and below 40°C which is a function of temperature and frequency but does not vary much with strain. The high damping was diminished only slightly when the material was commercially produced. These alloys were found to have very low strength, modulus and ductility when commercially cast. Although the heat treatment did not increase the damping it is possible that heat treating for a longer than 20 at 1350°C in helium would

increase the damping. The damping peaks are characteristic of an unidentified second order phase transformation like those found in shape memory alloys.

D. Future work

The damping mechanism should be determined. Efforts should be made to reduce the interstitial elements and break up the alpha phase in order to try to increase the toughness and damping capacity of alloys in this high damping system. Heat treatments of longer than 20 hours at 1350°C should be made to determine if they would further increase the damping.

Figure 17. Scanning Electron Micrographs of $Ti_{78}Sn_{22}$ Fracture Surface

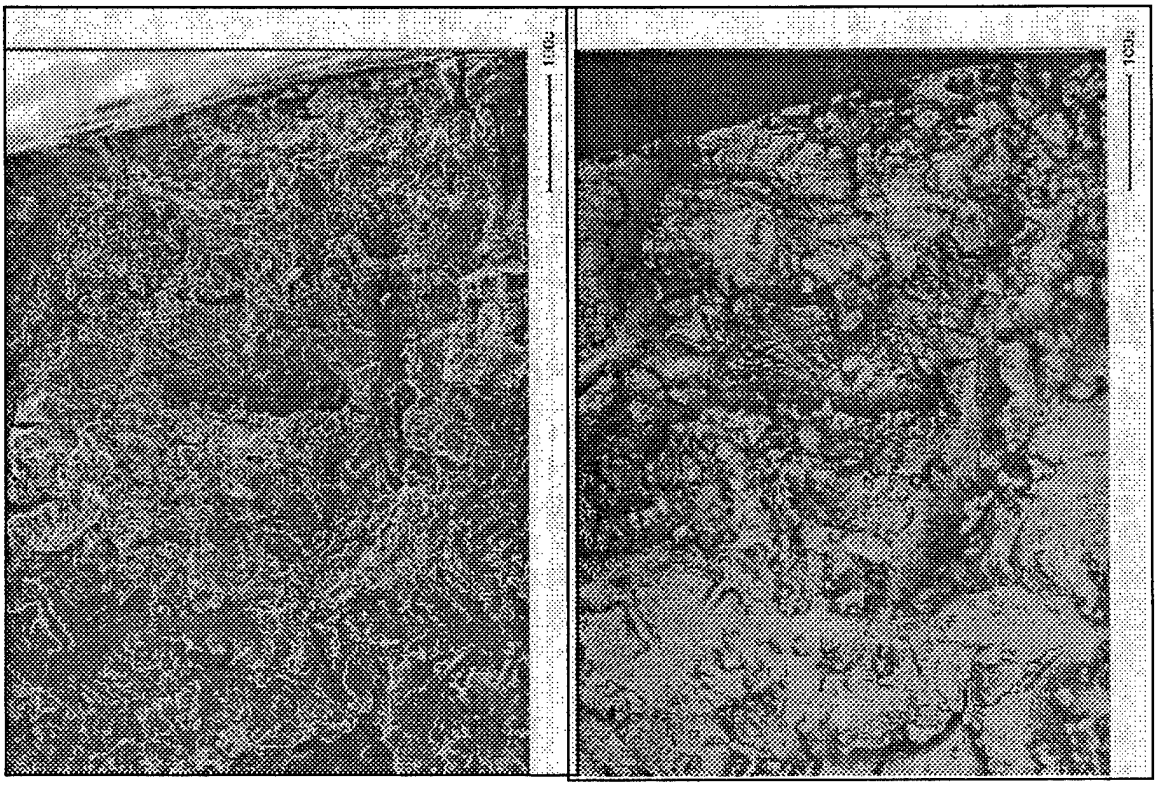

secondary electron image backscattered electron image

IV. MODIFIED CU-MN-AL HIGH DAMPING ALLOYS

A. Experimental procedure

1. Spray forming

The starting materials, consisting of a master alloy of 70-30 Cu-Mn with elemental additions made to achieve the desired chemistry, were melted in a nitrogen atmosphere. The master alloy was used instead of elemental Cu and Mn because the flake shape of the electrolytic grade Mn caused arcing in the melt during the initial attempts to spray form the alloy. The resulting melt was highly viscous and did not feed through the spray nozzle readily. The materials were sprayed in about 5 lb. heats at a temperature of 1035 °C using a nitrogen atmosphere.

2. Metallographic and EDS characterization

The chemical analyses, shown in Table 9, were obtained by inductively coupled plasma methods; while, analysis of selected areas was performed using energy dispersive spectroscopy (EDS) on polished and unetched samples.

Table 9. Results of Chemical Analysis of Bulk Samples in Weight Percent

Sample	Cu	Mn	Al	Zr	Er
Cu-Mn-Al	bal.	41.65	1.99	--	--
Cu-Mn-Al-Zr	bal.	40.30	2.45	0.307	--
Cu-Mn-Al-Er	bal.	42.09	2.51	--	0.11
Cu-Mn-Al-Zr-Er	bal.	41.84	2.51	0.38	0.22

The spray formed material was cut into approximately 1 x 10 x 60 mm blocks and solution treated at 800 °C 45 minutes in an argon atmosphere. They were then aged in the Polymer Laboratories Dynamic Mechanical Thermal Analyzer (DMTA) at 400 °C for 6 hours while damping measurements were continuously taken. The resulting material was underaged in order to magnify the strain aging effect[1].

Optical microstructural analysis was performed on samples which were polished and etched with Picral and Nital. Microstructural characterization was performed on the actual pieces used for the damping testing, except for the as sprayed condition. In that case, material adjacent to the samples was taken from the ingot.

ASTM grain size was measured from optical micrographs taken at 100x using a LECO 2001 Image Analyzer.

3. Damping

All samples were tested at three distinct alternating frequencies of vibration: 0.1, 1, and 10 Hz. The load applied during the bulk of the test was sufficient to impart a maximum strain of 10^{-4}. It is important to note that a much higher load was initially applied and then reduced until the proper displacement was achieved.

B. Results and discussion

1. Chemical, metallographic and EDS characterization

The bulk chemical analysis shows the composition to be close to that of Incramute in major alloying elements. The as-spray-formed material was not totally uniform. Cu rich

regions were found which have a composition (as measured by EDS) near the liquidus minimum shown in Figure 18. The black irregular inclusions, shown in micrographs in Figure 19, indicate that much of the aluminum oxidized and did not go into solution. The unmodified Cu-Mn-Al showed plate shaped silicon particles which did not dissolve during solution treating. Only a few areas high in Er were identified in the alloys which contained Er, but many fine white needle shaped particles of Zr were found in the alloys which contained Zr. Figure 20 shows that in the solution treated samples the areas high in copper and most of the Zr needles had dissolved into the matrix. The Al inclusions remained, and EDS analysis indicated that Er or Zr was often found in the same areas as Al in the alloys which contained those elements.

The grain size measurements, listed in Table 10 show that the grain size was initially very fine in the unmodified and Zr only addition alloys. After solution treatment all the alloys had essentially the same grain size.

2. Damping

Figure 21 shows that the damping capacity during aging at 400°C initially decreased for one or two hours then leveled out. The higher the gettering element content, the higher the damping during aging. The higher damping also correlated to the increased formation of alpha manganese at the grain boundaries as depicted in Figure 22.

Figure 18. Cu-Mn Phase Diagram [Ref. 17]

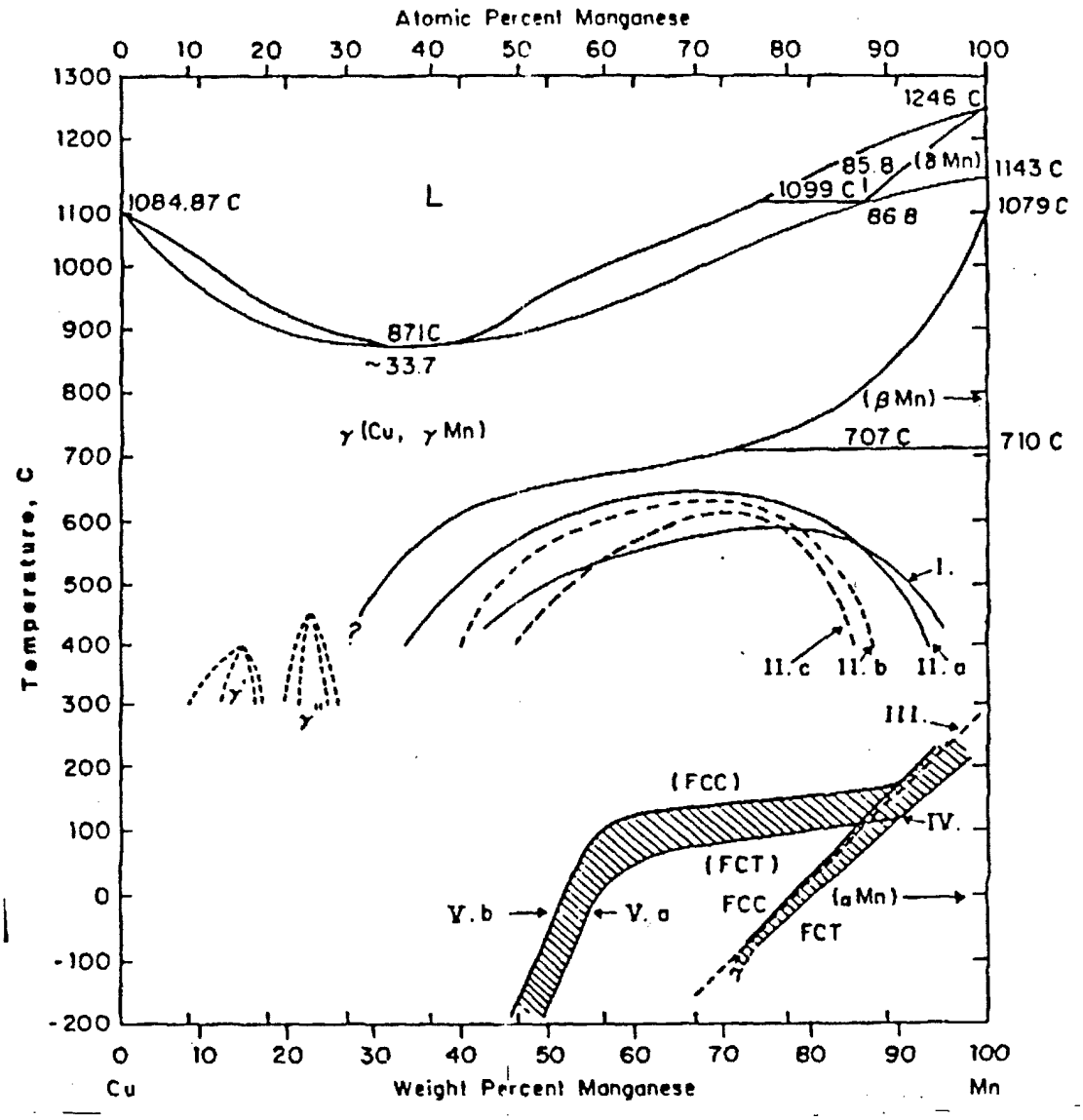

I. Miscibility Gap
II. Miscibility Gap
    a. Layering Range.
    B. Chemical Spinodal
    c. Coherent Spinodal
III. Neel Temperature
IV. FCC to FCT transition in quenched alloy
V. FCC to FCT transition in aged alloys

Figure 19. Optical Micrographs Of The As Spray Formed Material

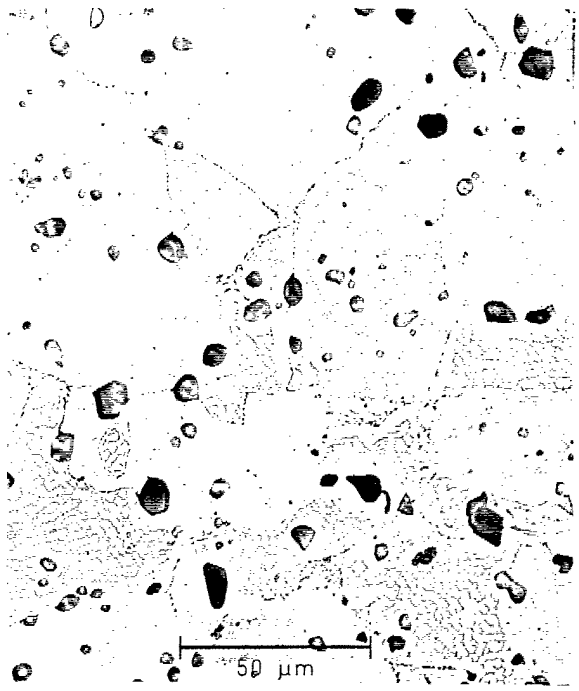

Cu-Mn-Al

Cu-Mn-Al-Zr

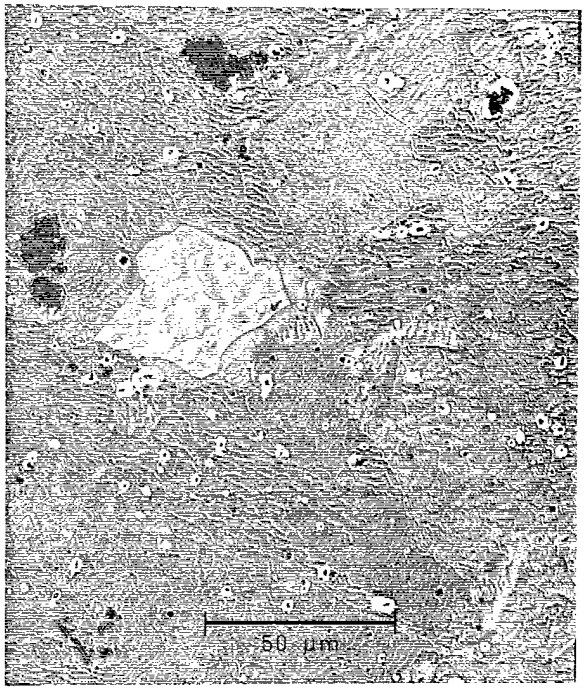

Cu-Mn-Al-Er

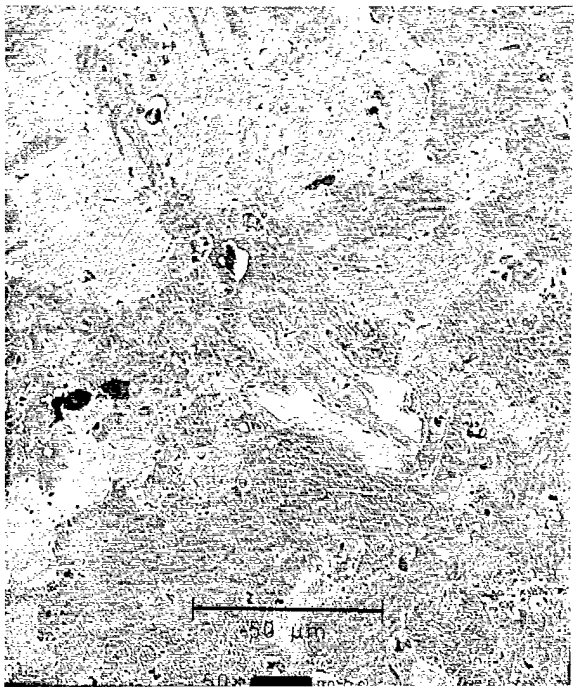

Cu-Mn-Al-Zr-Al

Figure 20. Optical Micrographs Of The Solution Treated Material

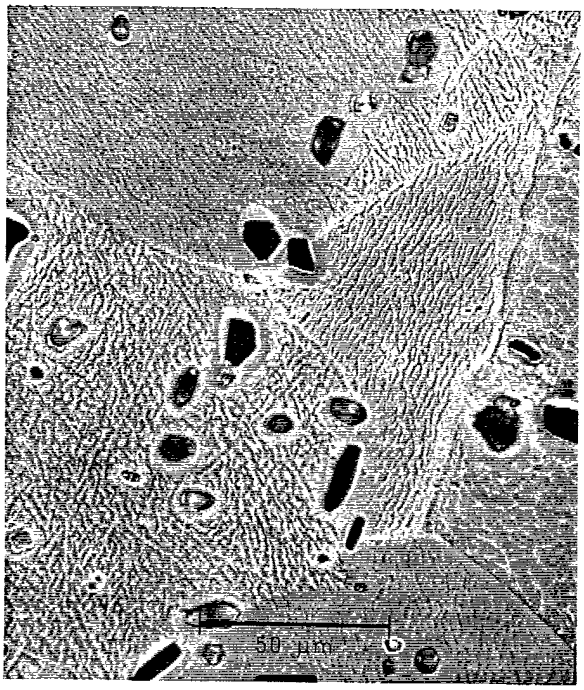

Cu-Mn-Al

Cu-Mn-Al-Zr

Cu-Mn-Al-Er

Cu-Mn-Al-Zr-Al

Table 10. ASTM Grain Size

Sample	As Spray Formed	Solution Treated	Aged
Cu-Mn-Al	9.6	5.0	5.2
Cu-Mn-Al-Zr	9.7	6.5	6.6
Cu-Mn-Al-Er	5.5	5.6	5.6
Cu-Mn-Al-Zr-Er	5.0	5.5	5.8

The damping data shown in Figure 23 illustrates the importance of continuous application of strain on the behavior of the material. In the alloys with the gettering additions, the damping was higher when the measurements were resumed after pausing for as little as 13 hours. This effect noticeably decreases over time and is not found in the unmodified alloy. The damping capacity plotted in Figure 24 corroborates the trend shown in Figure 23 with the damping capacity drastically increasing when the material was not tested for a week. Under the application of constant strain the solute elements diffuse to the area of the antiferromagnetic domain walls thus reducing their mobility. When samples are not vibrated, the mobile solute elements diffuse to the now stationary boundaries again reducing their mobility. This produces solute-rich and solute-poor regions. The initial large vibration breaks the boundaries free of the pinning elements and the walls traverse solute-poor regions, which results in higher damping. As long as there are mobile solute elements in the alloy, the damping capacity will change with time and vibrational strain history.

In all the modified alloys the damping decreased with time but the rate of decrease slowed with increasing content of gettering element. Although there is a lot of scatter in the data, it is evident that the alloy with the highest gettering content had the most

consistent damping level. The distance at which solute atoms can be attracted to a domain boundary is finite. Although the attraction is initially high, it falls over time as the solute becomes more dilute. Therefore the presence of mobile solutes can be determined by the stability of the damping capacity over time. It is evident from this data that the gettering elements were effective in reducing the amount of mobile solute elements.

C. Conclusions

The spray forming parameters have not been optimized and a large fraction of the aluminum and the gettering elements were not in solution. The sample containing zirconium exhibited the highest damping, and the sample containing the highest concentration of gettering elements was the most effective at maintaining high damping. This shows for the first time that zirconium is effective in increasing damping in this alloy system and lends support to the concept that the decrease in the damping capacity over time in Cu-Mn alloys is in fact due to the migration of solute elements to the domain walls.

D. Future work

Additional work is required to optimize the spray forming parameters in order to minimize the solute elements, reduce the oxidation of the alloying elements and increase the amount of the gettering elements in solution. The spray forming optimization must be done before the effect of the gettering elements can be accurately quantified.

Figure 21. Damping Capacity During Aging

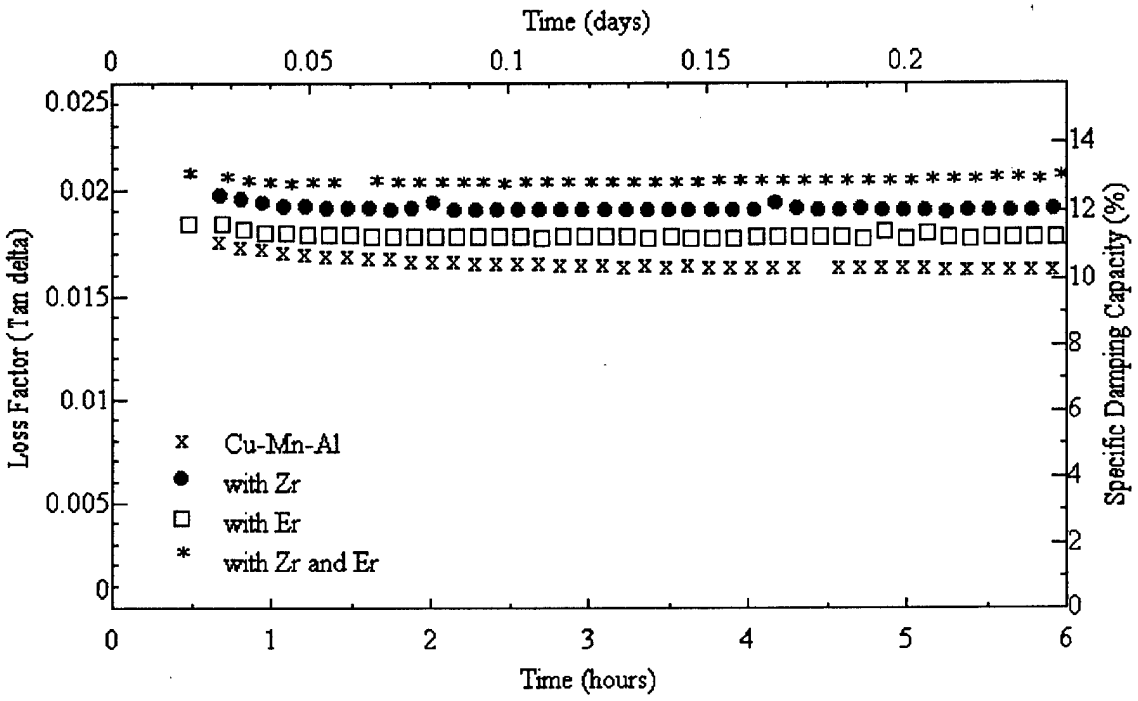

Figure 22. Optical Micrographs of the Aged Material

Cu-Mn-Al

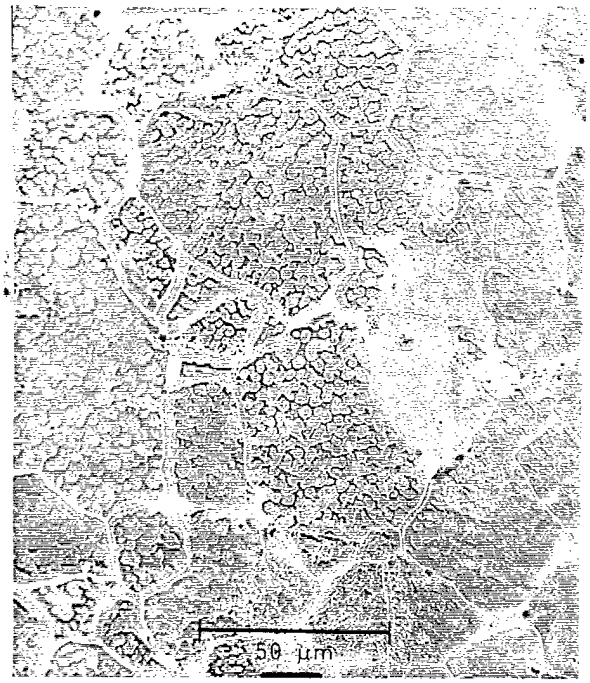

Cu-Mn-Al-Zr

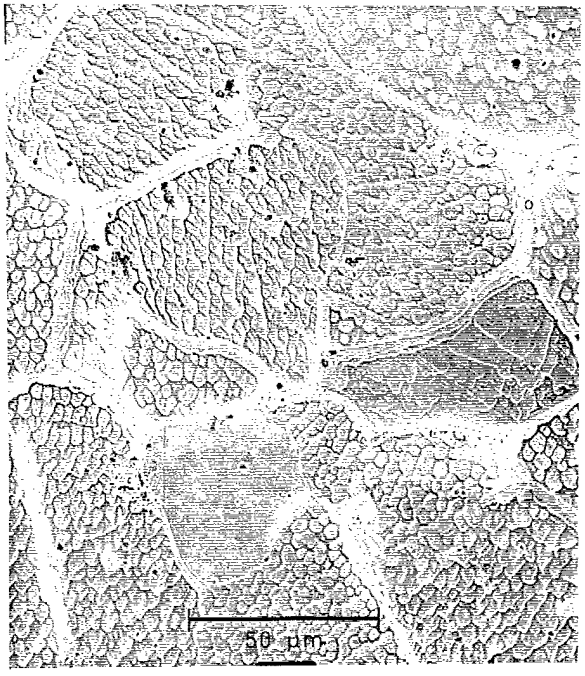

Cu-Mn-Al-Er

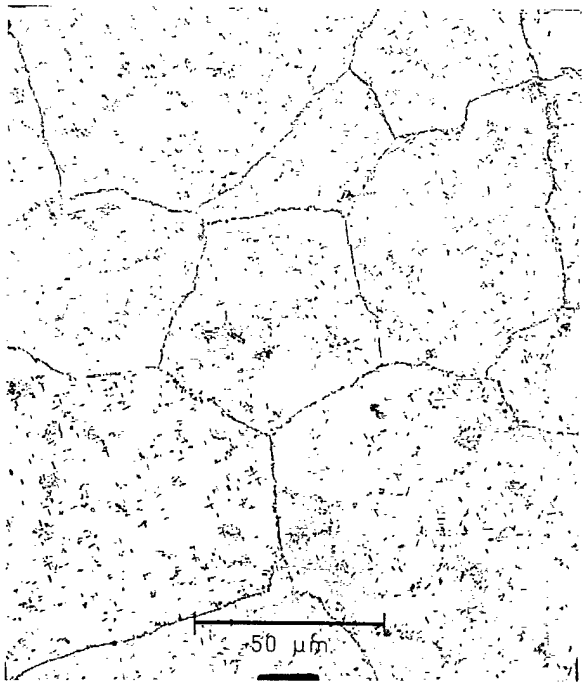

Cu-Mn-Al-Zr-Al

Figure 23. Damping Capacity The First Week After Aging

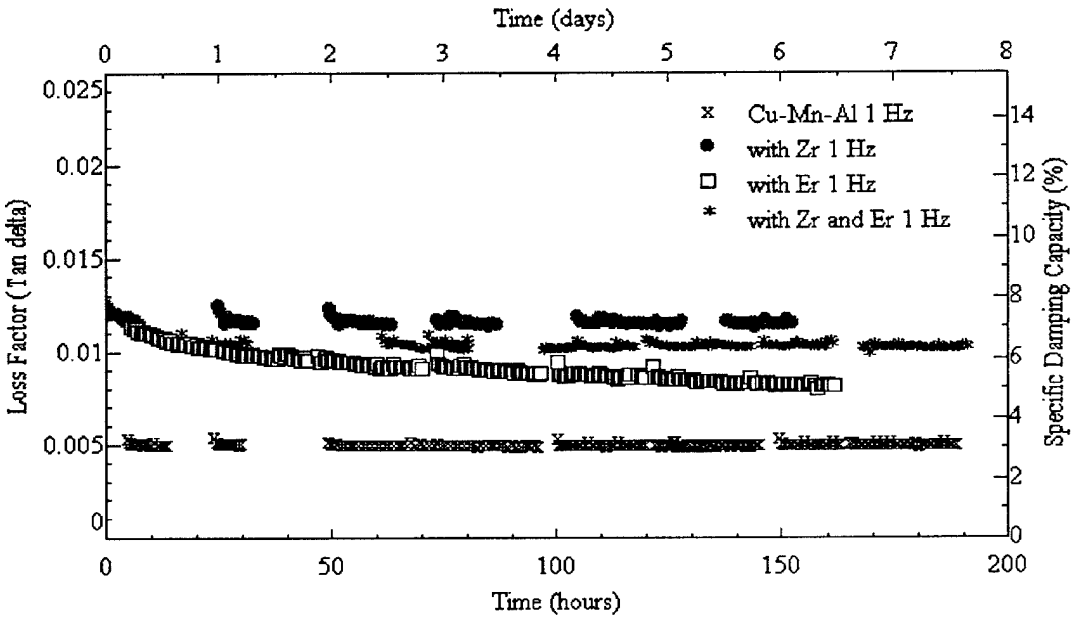

Figure 24. Damping Capacity Five Weeks After Aging

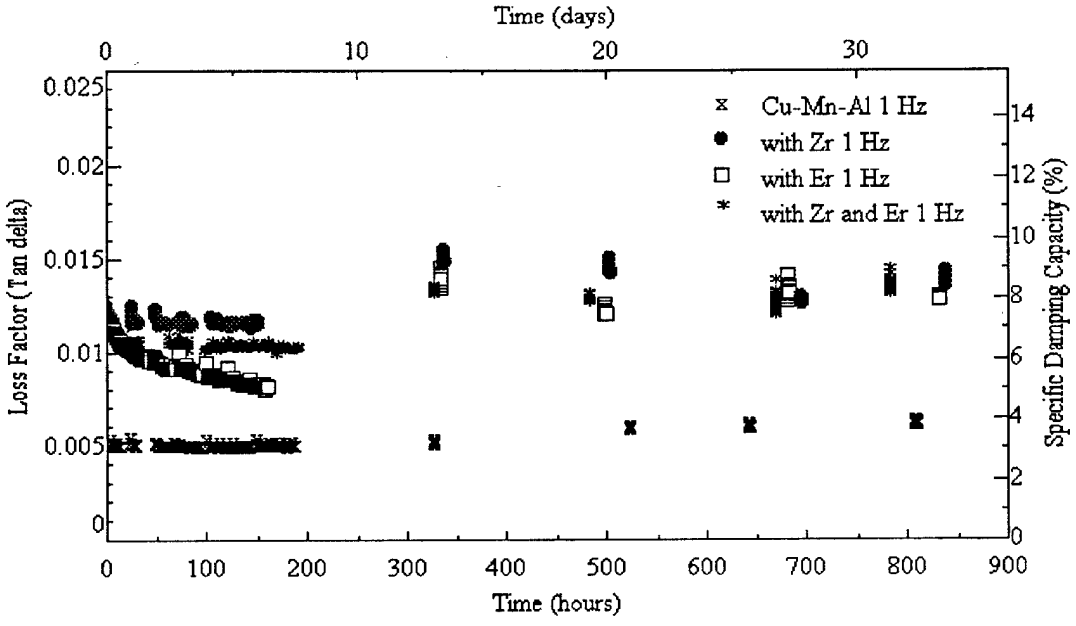

V. REFERENCES

1. Nashif, A.D., D.I.G. Jones, J.P. Henderson, *Vibration Damping* (John Wiley and Sons, New York, 1985)

2. Bert, C.W., "Material Damping: An Introductory Review of Mathematical Models, Measures and Experimental Techniques", Journal of Sound and Vibration 29, 129-153, (1973).

3. Nowick, A.S. and Berry, B.S., *Anelastic Relaxation in Crystalline Solids* (Academic Press, Inc., New York, 1972).

4. Shames, I.H. and Cozzarelli, F.A., *Elastic and Inelastic Stress Analysis*, (Prentice-Hall, Inc., New Jersey, 1991).

5. Lazan, B.J., *Damping of Materials and Members in Structural Mechanics*, (Pergamon Press, NY, 1968).

6. Soovere, J. and M.L. Drake, "Aerospace Structures Technology Damping Design Guide Volume 1 - Technology Review", AFWAL - TR - 84 - 3089 (Dec 1985).

7. Biot, M.A., U.S. Nat. Cong. of App. Mech., 1 (1958).

8. Rao, J.G. and S Ankem, "The Effect of Volume Percent and Morphology of Phases on the Damping Behavior of Epoxy/Aluminum Composites", Metallurgical and Materials Transactions 27A, 2366 (1996).

9. Fleischer, R.L., R.S. Gilmore, and R.J. Zabala, J. Appl. Phys. 64, 2964 (1988).

10. Fleischer, R.L., and R.J. Zabala, Metallurgical Trans. 21A, 1951 (1990).

11. Nachman, J.F., J.C. Napier and A.N. Hammer, "Development of Cu-Mn Base Alloys with High Damping Properties", Final report, April 1, 1970 to March 31, 1971, INCRA Project No. 152A.

12. Ritchie, I.G., Z-L. Pan, D.W. Sprungmann, H.K. Schmidt and R. Dutton, "High Damping Alloys - The Metallurgist's Cure for Unwanted Vibrations", Canadian Metallurgical Quarterly, (1987).

13. Sahoo, M., G. Crawford, and J.R. Barry: "Foundry Characteristics and Mechanical Properties of a High-Damping Propeller Alloy.", Energy Mines and Resources Canada Report, MRP/PMRL 83-59 (OP-J), (1983).

14. Anderson, I.E., R.A. Masumura, B.B. Rath, and C.L. Vold, " Structure and Properties of RSP Copper-Based Alloys", Proceedings of the Third Conference On Rapid Solidification Processing held at NBS Gaithersburg MD, 178-185 (Dec 1982).

15. Ross, B.A. and D.C. Van Aken: Scripta Metallurgica, 23, 2085-2090 (1989).

16. Schetky, L. and D. Peters, "The Damping Properties of Copper-Manganese Alloys.", Proceedings of the Role of Interfaces on Material Damping, ASM, , 73-79 (1985).

17. Holsten, G.V., "Phase Transformations and Microstructural Evolution in Aged Mn-Cu-Based Alloys", Master Thesis, Naval Postgraduate School, Monterey CA, (June 1990).

INITIAL DISTRIBUTION

Copies	
1	ONR Code 332 (Kabacoff)
1	NAVPGSCOL Code 69Ps (Perkins)
2	DTIC

CENTER DISTRIBUTION

Copies	Code	Name
1	60	(Wacker)
1	601	(Morton
1	603	(Cavalaro)
1	609	(Malec)
1	61	(Holsberg)
1	612	
5	612	(CRW)
1	3442	(TIC)